REPUBLIC OF TURKEY

YILDIZ TECHNICAL UNIVERSITY

GRADUATE SCHOOL OF SCIENCE AND ENGINEERING

COMPARISON OF POLLUTANT DISPERSION BY USING AERMOD AND CFD MODELS

Elif YAVUZ

MASTER OF SCIENCE THESIS

Department of Environmental Engineering

Environmental Engineering Program

Advisor

Assoc. Prof. Dr. S. Levent KUZU

July, 2021

REPUBLIC OF TURKEY

YILDIZ TECHNICAL UNIVERSITY

GRADUATE SCHOOL OF SCIENCE AND ENGINEERING

COMPARISON OF POLLUTANT DISPERSION BY USING AERMOD AND CFD MODELS

A thesis submitted by Elif YAVUZ in partial fulfillment of the requirements for the degree of MASTER OF SCIENCE is approved by the committee on 07.07.2021 in Department of Environmental Engineering, Environmental Engineering Program.

Assoc. Prof. Dr. S. Levent KUZU

Yildiz Technical University

Advisor

Approved By the Examining Committee

Assoc. Prof. Dr. S. Levent KUZU, Advisor
Yildiz Technical University _____

Prof. Dr. Arslan SARAL, Member
Yildiz Technical University _____

Prof. Dr. Tayfun KINDAP, Member
Istanbul Technical University _____

I hereby declare that I have obtained the required legal permissions during data collection and exploitation procedures, that I have made the in-text citations and cited the references properly, that I haven't falsified and/or fabricated research data and results of the study and that I have abided by the principles of the scientific research and ethics during my Thesis Study under the title of comparison of pollutant dispersion by using AERMOD and CFD models supervised by my supervisor, Assoc. Prof. Dr. S. Levent KUZU. In the case of a discovery of false statement, I am to acknowledge any legal consequence.

Elif YAVUZ

Dedicated to my family

and my friends

ACKNOWLEDGEMENTS

First and foremost, I have to thank my advisor Assoc. Prof. Dr. S. Levent KUZU for providing me with the support and direction to complete this work. I would like to thank Prof. Dr. Güleda ENGİN for her guidance and advices. I want to thank my family and friends for always being there and supporting me through everything.

Elif YAVUZ

TABLE OF CONTENTS

LIST OF SYMBOLS vii

LIST OF ABBREVIATIONS viii

LIST OF FIGURES ix

LIST OF TABLES x

ABSTRACT xi

ÖZET xiii

1 INTRODUCTION 1

1.1 Literature Review 1

1.2 Objective of The Thesis 3

1.3 Hypothesis 3

2 AIR POLLUTION 5

2.1 Air Pollution Sources 5

2.1.1 Natural Sources 5

2.1.2 Anthropogenic Sources 6

2.2 Air Quality Regulation in Turkey 6

3 AIR POLLUTION MODELLING 8

3.1 Modelling Methods 8

3.2 Dispersion Modelling 9

3.2.1 Box Models 11

3.2.2 Gaussian Plume Model 11

3.2.3 Eulerian Model 12

3.2.4 Lagrangian Model 12

4 MATERIALS AND METHODS 13

4.1 General Characteristics of The Study Region 13

4.2 Source Stacks 14

4.3 Air Quality Monitoring Station (AQMS) 15

4.4 Meteorology Station 16

4.5 AERMOD 18

4.5.1 Model Domain and Topography 19

4.5.2 AERMET Preprocessor 20

4.6 Weather Research and Forecasting Model (WRF) 22

4.6.1 WRF Model Setup 23
4.7 WRF Model Results Verification Methodology 24
4.8 Computational Fluid Dynamics (CFD) 25
5 RESULTS AND DISCUSSION 31
5.1 Weather Research and Forecast (WRF) Model Results 31
5.1.1 WRF Verification Results 32
5.2 AERMOD Model Results 33
5.3 CFD Model Results 35
5.4 CFD and AERMOD Model Results Comparison 40
6 CONCLUSION 44
REFERENCES 45
A WPS INPUT 49
B WRF INPUT 50
PUBLICATIONS FROM THE THESIS 53

LIST OF SYMBOLS

u	The average wind speed in the x-direction
r	The coefficient of correlation
H	The effective stack height
N	The number of data
O	The observed data
C	The pollutant concentration
Q	The pollutant emission rate
P	The predicted data
σy	The standard deviation of the beam in y direction
σz	The standard deviation of the beam in z direction

LIST OF ABBREVIATIONS

ANN	Artificial Neural Network
AQMS	Air Quality Monitoring Station
AQI	Air Quality Index
CFD	Computational Fluid Dynamics
DMM	Deterministic Mathematical Models
FB	Fractional Bias
IOA	Index of Agreement
MB	Mean Bias
NAQMN	National Air Quality Monitoring Network
NE	North East
NNE	North North East
PBL	Planetary Boundary Level
PM	Particulate Matter
RMSE	Root Mean Square Error
SE	South East
SO_2	Sulphur dioxide
SW	South West
UTM	Universal Transverse Mercator
WRF	Weather Research and Forecasting
WPS	WRF Pre-Processing System

LIST OF FIGURES

Figure 3.1 Air quality model classification 9
Figure 3.2 Dispersion modelling key steps 10
Figure 3.3 The model that can be applied depending on the complexity of the task 11
Figure 4.1 The map of Çanakkale where the study area is located 13
Figure 4.2 Biga-İçdaş thermal power plant source stacks, AQMS, meteorology station. 15
Figure 4.3 Biga-İçdaş AQMS daily observed SO_2 concentrations ($\mu g/m^3$) 16
Figure 4.4 Daily observed temperature results at Biga-Kemer Köyü ground level meteorology station for the year 2014 17
Figure 4.5 Wind rose diagram at Biga-Kemer Köyü ground level meteorology station for the year 2014 17
Figure 4.6 The schematic of Gauss dispersion model refers to a single point source 18
Figure 4.7 AERMOD model domain topography 19
Figure 4.8 AERMET data processing procedure 20
Figure 4.9 Weather Research and Forecasting (WRF) model flow chart 22
Figure 4.10 WPS and WRF Flow 23
Figure 4.11 WRF Model outer (blue line) and inner (red line) area boundaries 24
Figure 4.12 CFD process steps 26
Figure 4.13 Three dimensional geometry of the study area 28
Figure 4.14 The view of the Case 1 three-dimensional terrain on the meshing interface 29
Figure 5.1 The predicted (WRF) and observed (Biga-Kemer Köyü station) daily temperature values 31
Figure 5.2 The wind rose diagram for the year 2014 obtained from the WRF model 32
Figure 5.3 The relation between actual measurement temperature results and WRF model results for the year 2014 33
Figure 5.4 The annual (a) 24-hr maximum (b) and hourly maximum (c) SO_2 concentrations ($\mu g/m^3$) distribution plots for the year 2014 34
Figure 5.5 The CFD iso-surface plots based on SO_2 mass fraction for all cases 38
Figure 5.6 Velocity streamline at different surface properties (a) for flat terrain (b) for elevated terrain 40

LIST OF TABLES

Table 2.1 Limit values, maximum number of exceeds allowed in one year and tolerance marjin in the air quality assessment and management regulation 7

Table 4.1 Biga-İçdaş thermal power plant stack properties 14

Table 4.2 The land use parameters used in the preprocessor of AERMET 21

Table 4.3 Physical Parameterizations used in WRF Model 24

Table 4.4 The cases used in CFD Model Simulations 28

Table 5.1 Verification results for the daily average temperature values 32

Table 5.2 Comparison of Measurement and CFD and AERMOD estimated SO_2 concentration results 41

ABSTRACT

COMPARISON OF POLLUTANT DISPERSION BY USING AERMOD AND CFD MODELS

Elif YAVUZ

Department of Environmental Engineering

Master of Science Thesis

Advisor: Assoc. Prof. Dr. S. Levent KUZU

Many atmospheric contaminants such as CO_2, SO_x, NO_x, and particulate matter (PM) are released into the atmosphere through the burning of fossil fuels, resulting in high levels of air pollution. In this study, the dispersion of SO_2 from a coal fired power plant power was simulated using AERMOD and CFD models that use different approaches for the prediction of pollutant concentrations. The closest meteorological station data were prepared by using AERMET preprocessor of AERMOD and the missing temperature and cloud cover data were completed with using Weather Research and Forecasting (WRF) prognostic model. The air quality monitoring station was described as the receptor point and AERMOD model was run for the year 2014 to obtain hourly maximum, daily maximum, and annual ground level SO_2 concentrations. The CFD model was run for seven cases with varying wind speeds and PBL heights computed using AERMET, by determining critical speed wind direction that the wind blows directly from the source stacks toward AQMS. The findings from these two approaches were compared with each other and with the observed values, and models performances were assessed.

Between two models, the concentration values downwind of the source differ significantly. In both models, meteorological conditions, especially PBL, had a significant impact on calculated downwind SO_2 concentrations. CFD calculated lower downwind

concentrations for all seven cases compared to AERMOD and observation values. AERMOD predicted higher values in four cases and lower values in three cases compared to observation values. When hypothetical flat terrain is used, the estimation results of two models got closer. The main difference in determining the concentration is the Eulerian approach of CFD. Therefore, for single case runs CFD dispersion is recommended according to our results.

Keywords: AERMOD, CFD, dispersion

ÖZET

AERMOD ve CFD Modelleri Kullanılarak Kirletici Dağılımının Karşılaştırılması

Elif YAVUZ

Çevre Mühendisliği Bölümü

Yüksek Lisans Tezi

Danışman: Doç. Dr. S. Levent KUZU

CO_2, SO_x, NO_x ve partikül madde (PM) gibi birçok atmosferik kirletici, fosil yakıtların yakılması yoluyla atmosfere salınır ve bu da yüksek düzeyde hava kirliliğine neden olur. Bu çalışmada, kirletici konsantrasyonlarının tahmini için farklı yaklaşımlar kullanan AERMOD ve CFD modelleri kullanılarak kömürle çalışan bir elektrik santralinden SO_2 dağılımı simüle edilmiştir. En yakın meteoroloji istasyonu verileri, AERMOD'un AERMET ön işlemcisi kullanılarak hazırlanmış ve eksik sıcaklık ve bulut kapalılığı verileri, Weather Research and Forecasting (WRF) prognostik modeli kullanılarak tamamlanmıştır. Hava kalitesi izleme istasyonu alıcı nokta olarak tanımlanmış ve saatlik maksimum, günlük maksimum ve yıllık yer seviyesi SO_2 konsantrasyonlarını elde etmek amacıyla 2014 yılı için AERMOD modeli çalıştırılmıştır. CFD modeli, rüzgarın doğrudan kaynaktan AQMS'e doğru estiği kritik hız rüzgar yönü belirlenerek, AERMET kullanılarak hesaplanan değişken rüzgar hızları ve PBL yükseklikleri ile yedi durum için çalıştırılmıştır. Bu iki yaklaşımdan elde edilen bulgular birbirleriyle ve gözlenen değerlerle karşılaştırılarak modellerin performansları değerlendirilmiştir.

İki model arasında, kaynağın rüzgar altı konsantrasyon değerleri önemli ölçüde farklılık göstermiştir. Her iki modelde de meteorolojik koşullar, özellikle PBL, hesaplanan rüzgar

altı SO_2 konsantrasyonları üzerinde önemli bir etkiye sahiptir. CFD, AERMOD ve gözlem değerlerine kıyasla yedi vakanın tümü için daha düşük rüzgar altı konsantrasyonları hesaplamıştır. AERMOD, gözlem değerlerine kıyasla dört durumda daha yüksek ve üç durumda daha düşük değerler öngörmüştür. Varsayımsal düz arazi kullanıldığında, iki modelin tahmin sonuçları birbirine yaklaşmıştır. Konsantrasyonun belirlenmesindeki temel fark, CFD'nin Euler yaklaşımıdır. Bu nedenle, sonuçlarımıza göre tek vaka çalışmaları için CFD dağılımı önerilmiştir.

Anahtar Kelimeler: AERMOD, CFD, dispersiyon

1
INTRODUCTION

1.1 Literature Review

Today's rapid population growth, urban and industrial development, increased fuel usage, and chemical use results in the release of a variety of pollutants into the atmosphere that cause air pollution (Arya, 1999). The high level of air pollution was caused by the presence of pollutants resulting from various activities, especially those in the industrial and transportation sectors (Li ve et al, 2010).

Fossil fuel combustion is one of the primary cause of ambient air pollution. It's known that huge quantities of carbon dioxide (CO_2), sulphur dioxides (SO_x), nitrogen oxides (NO_x), and particulate matter (PM) are released into the atmosphere during the combustion of fossil fuels (Singh et al., 2020; Lee & Zhou, 2015; Nam et al., 2013; Omidvarborna et al., 2015; Streeter, 2016). These emissions are hazardous for both human health and environment. It is known that even exposure to pollutant thresholds value has negative consequences for human health (Zou et al., 2009).

Sulfur dioxide (SO_2) is primarily generated by power plants that burn coal to generate electricity. At room temperature, it is a colorless, non-flammable gas. It is one of the six classic air pollutants listed by the American Environmental Protection Agency (US-EPA). It is harmful to both human health and the climate. It can cause stroke, cancer and cardiovascular diseases, as well as respiratory illnesses such as asthma which can lower lung capacity (WHO, 2016; EEA (European Environment Agency), 2014). It also leads to acid deposition, which can have serious consequences for forests and rivers and lakes ecosystems.

It is very important to develop and implement an effective air quality management in order to protect public and environmental health from the negative effects of air pollution (MARKA, 2012). Air pollution modelling is a critical stage of designing an air pollution control strategy. Although air quality monitoring stations provide

only a limited amount of data, air pollution modelling allows researchers to know pollutant levels, behaviors and future trends in ambient environment (Thi Nguyen & Kim, 2006).

Deterministic models, statistical models and physical models are the most common modelling methods used in air pollution studies. There are various kinds of models to simulate the dispersion of pollutants that developed by US EPA. AERMOD is one of the recommended steady state plume model that can effectively being used up to 50 km radius.

In cases where the meteorological data required to initialize the AERMOD model are not available, the AERMOD model can be coupled with the Weather Research and Forecasting (WRF) prognostic model. The WRF model calculates three dimensional meteorological parameters (wind speed and direction, temperature, pressure, humidity, precipitation etc.) on the basis of Navier-Stokes equations. In the literature, there are several studies presented the application of AERMOD-WRF models to simulate the dispersion of pollutants (Malakan et al., 2018; Kesarkar et al., 2007; Kumar et al., 2017).

Although AERMOD model has major advantages in terms of processing time, ease of use and cost, the lack of in-program fluid flow modelling, as well as the grid size and resolution constraints, limit the AERMOD model. On the other hand, computational fluid dynamics (CFD) is a suitable tool for modelling pollutant dispersion where grid size and resolution can be manually adjusted depending on need and accuracy. It is based on fluid mechanics principles and uses the Navier-Stokes equations. It employs computational methods and algorithms to solve the problems.

In this thesis, SO_2 emission dispersion modelling from a coal fired thermal power plant was simulated using AERMOD and CFD models and the missing meteorological data was generated with WRF model. This thesis includes the comparison of Eulerian and Gaussian approaches for a pollutant dispersion.

1.2 Objective of The Thesis

In general, the purpose of this thesis is to assess the model performances by predicting ground level pollutant concentration based on SO_2 data of a coal fired thermal power plant. The objectives of the thesis are:

i. To predict ground level SO_2 concentration from a coal fired thermal power plant and to investigate the dispersion of SO_2 in the study area by using two models that have different approaches
ii. To provide missing meteorological data for the AERMOD model using Weather Research and Forecasting (WRF) prognostic model
iii. To compare the results of the two models with the AQMS data and assess the model's efficiency.

1.3 Hypothesis

The aim of this study is to model the dispersion of SO_2 emissions from a thermal power plant in Çanakkale, Turkey. It includes the prediction of ground level SO_2 concentration through AERMOD and CFD models, which have different approaches as well as comparing the model results with air quality monitoring station (AQMS) that defined as the receptor point.

This current study suggest the use of CFD as a numerical alternative to AERMOD where the dispersion of pollutants calculated using Gaussian plume model. One of the most important features of this study is the 3D terrain integration into the CFD model. In this way, the impact of terrain on wind flow and dispersion of pollutants were analyzed with CFD model simulations. The performances of both models were determined by running the CFD model for the days when the wind blows directly to the AQMS and comparing the CFD simulation results with the AQMS data and the results of the AERMOD model.

The study reveals the possible effects of air pollution of the Biga-İçdaş thermal power plant in the study area. It is the first attempt to use the WRF prognostic model integrated with AERMOD dispersion model applied for the Biga region. This research provides a better understanding of SO_2 dispersion in complex terrain using two different models that have different approaches. The study will be an

important input for future studies. It will be useful in the future for the enforcement of local ambient air quality requirements, as well as the study's rich data will increase awareness and close the gap in this field.

2
AIR POLLUTION

Air pollution can be described as the presence of substances in the form of solid, liquid, that may be harmful to human health, living life, and ecological balance by disrupting the natural composition of the air. Air pollution is one of the most serious environmental issues. After being released into the atmosphere, it can spread to large areas in a short time and can remain in the atmosphere. It is known that particulate pollutants have a short lifespan, ranging from a few days to several weeks, on contrast, gas pollutants have a residence period from a few seconds to hundreds of years (Seinfeld and Pandis, 2006). Air pollution has many different types of sources.

2.1 Air Pollution Sources

Two main groups analyze the causes of air pollution, taking into account their basic characteristics. There are natural air pollution sources and anthropogenic air pollution sources. Natural activities release a significant amount of contaminants into the atmosphere. Air pollution, on the other hand, is mainly caused by anthropogenic sources rather than natural sources.

2.1.1 Natural Sources

Natural causes of air pollution are contaminants that arise as a result of natural activities and have no human impact. Natural sources that cause air pollution are can be listed as;

- Volcanoes
- Forest fires
- Windblown dust
- Sea salt spray
- Evaporation and biogenic activities

Large quantities of dust and gas, especially SO_2 and CO_2, are released into the atmosphere by volcanoes. Also forest fires release huge quantities of CO, CO_2, NO_X,

hydrocarbons and trace gases into the atmosphere. Forest burning may be caused by humans or by natural impacts, such as lightning. It is known that one of the most significant sources of suspended particulate matter is forest fires. Also thick sand deposits that can be carried by the winds in desert areas are one of the greatest sources of particles. They can be moved over long distances in this way. Formations in the form of salt sprays on oceans and seas transported to the atmosphere through evaporation and winds, resulting air pollution. Evaporation from the ocean and large water surfaces transfers the majority of trace gases to the atmosphere, and gases generated by biogenic activities are also natural sources of air pollution (Arya, 1999; Chambers, 2013).

2.1.2 Anthropogenic Sources

Anthropogenic sources are human activities that cause pollutant gas and particulate emissions. Anthropogenic resources are divided into two as "stationary sources" and "mobile sources". Stationary sources includes sources where pollutants generated during any production process by burning solid, liquid and gaseous fuels are emitted to the atmosphere through a stack. Some of these are power plants, industrial facilities, oil refineries, fuels used for heating in houses. The most important causes of air pollution are the heating process, production of hot water and steam in industry, and burning of fossil fuels for electrical energy generation in thermal power plants. Mobile sources are the pollutants originating from land, sea and air transport. In transportation, fuels such as diesel, gasoline or jet fuel are consumed, and the air pollutants released into the atmosphere from the exhausts of vehicles and cause air pollution similar to the combustion products formed by the burning of solid, liquid and gas fuels (Arya, 1999; (Henderson-Sellers, 1984).

2.2 Air Quality Regulation in Turkey

The monitoring of air quality and air pollution measurement studies in Turkey began with the Air Quality Control Regulation which entered into force in 1986. The mentioned regulation implemented by the Ministry of Health Sanitation Institute for many years and the air quality monitoring obligation has passed to the Ministry of Environment and Urbanization in 2005 (Gemici et al., 2017).

The Air Quality Assessment and Management Regulation, which is valid for the protection of air quality today, entered into force in the Official Gazette with the number 26898, dated 06.06.2008. Turkey has taken as targets EU limit values for air quality limit values. A certain period of time is defined as a transition period to reach desired levels. As of January 1, 2014, it is expected to meet EU limits for all pollutants by 2024, by calculating limit values for that year and progressively decreasing tolerance margins per year. Turkey will reach the NO_2 limit value in 2024 and will apply the EU legislation for all pollutants from this date. The assessment limits determined for the SO_2 pollutant according to the Regulation were given in Table 2.1 (HKDYY, 2008).

Table 2.1 Limit values, maximum number of exceeds allowed in one year and tolerance marjin in the air quality assessment and management regulation (HKDYY, 2008)

Parameter	**Period**	**Limit value (µg/m³)**	**Maximum number of excesses allowed in a year**	**Tolerance margin**				
				2014	2015	2016	2017	2018
SO_2 (µg/m³)	Hourly[1]	350	24	150	120	90	60	30
	Daily[1]	125	3	125	100	75	50	25
	Annual[2]	20	-	-	-	-	-	-

1: For the protection of human health

2: For the protection of ecosystems and vegetation

3
AIR POLLUTION MODELLING

The most critical stage of designing an air pollution control strategy is air pollution modelling to control air pollution on a local or regional scale. Air pollution modelling is required to improve field knowledge and accurately estimation of pollutant concentrations (Karatzas & Kaltsatos, 2007). Air quality models are used to illustrate the statistical association between pollutant emissions and pollutant concentrations in the ambient air. They are frequently used in modelling primary pollutant sources such as SO_x, CO, NO_x and VOC. The results of air pollution models are used in Environmental Impact Assessment reports of polluting sources, in determining the criteria for the location and planning of industrial facilities, determining the minimum stack height, developing and planning air quality control strategies, determining short term or long term measures to improve air quality. It can also be used for direct transmission of air quality information to the public.

3.1 Modelling Methods

There are many ways to categorize the variety current models based on their particular characteristics including; source-receptor relationship, model structure, frame of reference, dimension, scale, model structure, terrain and level of sophistication (Sharma et al., 2004). The most common modelling methods used in the study of air pollution are classified into three groups which are deterministic models, statistical models and physical models (Figure 3.1). The statistical models such as Artificial Neural Network (ANN) use statistical methods to determine concentrations from meteorological and pollutant parameters after achieving an effective statistical relationship empirically from calculated concentrations. In physical modelling such as wind tunnel modelling, a real process is simulated on a smaller scale in the laboratory with a physical experiment that models the original processes. Deterministic mathematical models (DMM) like AERMOD use the solutions of various equations that describe the related physical processes to

determine pollutant concentrations from pollution inventories and meteorological variables.

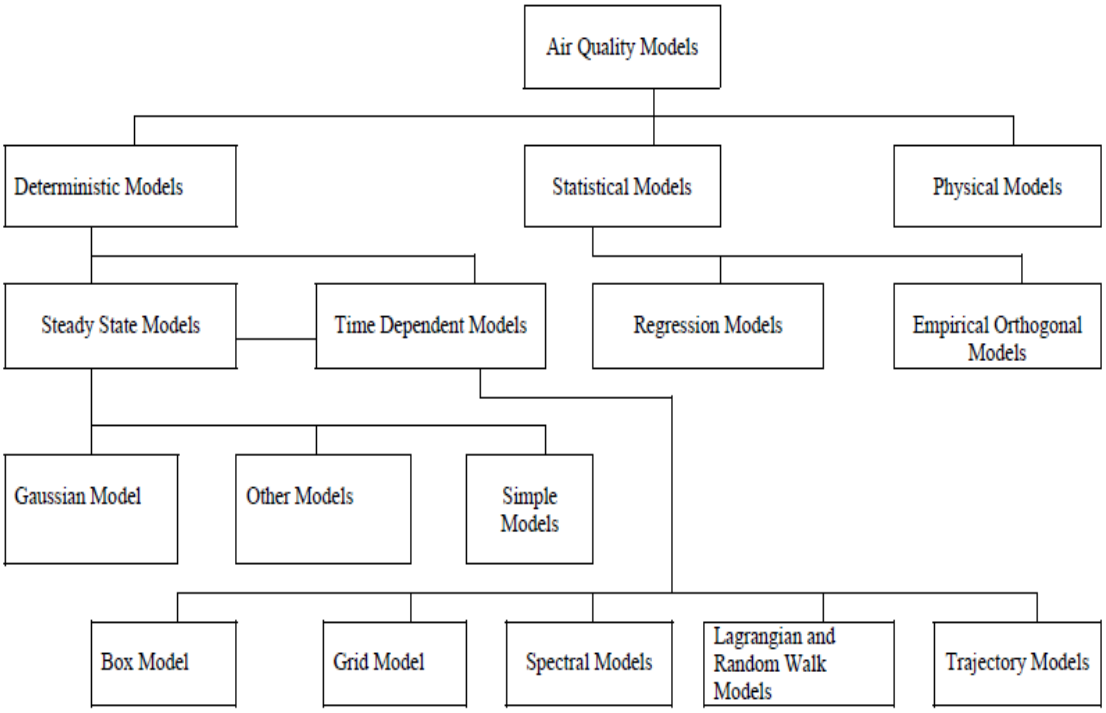

Figure 3.1 Air quality model classification (Weber, 1982)

3.2 Dispersion Modelling

Prevalent meteorological conditions such as wind profile, temperature profile, and atmospheric stability monitor the dispersion and emission of contaminants into the air. The interrelationships of these variables are attempted to be represented mathematically in air pollution dispersion models (Sinha et al., 2004). The downwind concentration of contaminants released by various emission sources, such as industrial facilities and public traffic, is calculated with the help of air dispersion models that solve mathematical equations and algorithms.

Figure 3.2 illustrates the four key steps in the air pollution dispersion modelling process. At first step background concentrations of pollutants, meteorological conditions, source data, model options (receptor grid and dispersion parameters) and local topographical features are specified. Then the ground level concentrations of pollutants calculated with the help of atmospheric dispersion

models. At last step the data are analyzed for the potential environmental and health effects. In each step of the process all errors taken into account.

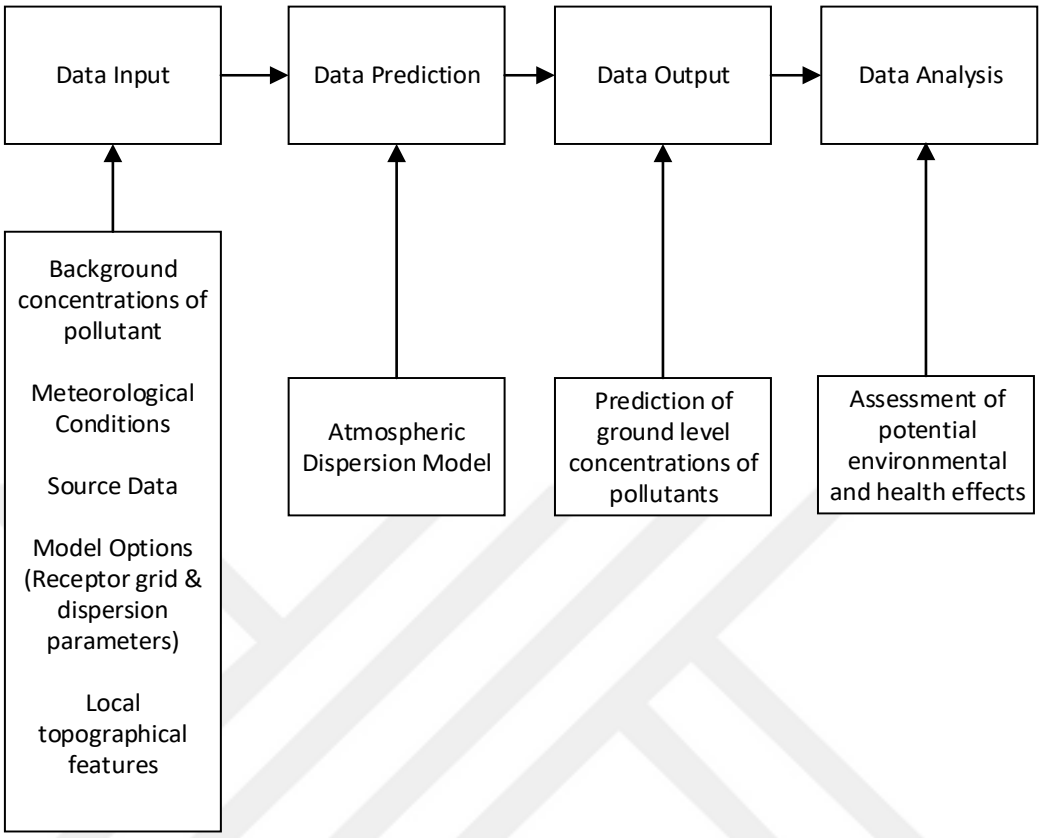

Figure 3.2 Dispersion modelling key steps (Bluett et al., 2004)

While there are many prospective applications of dispersion models, there are uncertainties that should always be taken into account, due to the lack of accurate source information, meteorological data, and the suitability of the chosen model. Although there are no rules for choosing dispersion models, it is well known that some models perform better than others in specific applications. Figure 3.3 gives information about the model that can be applied depending on the complexity of the problem. For low complexity modelling rarely required. When the complexity increases Gaussian plume models can be used. At cases when the complexity is high, Eularian and Lagrangian models can be applied with the help of advanced programs according to the specific tasks (Bluett et al., 2004). Today, EPA approved models are preferred to use in air quality modelling studies. EPA recommends steady-state Gaussian dispersion models such as SCREEN3, ISCT3, ISC-PRIME and AERMOD dispersion models for modelling a region with a radius less than 50 km

while for modelling a region with a radius of more than 50 km the unstable Lagrangian PUFF dispersion model CALPUFF is recommended (US-EPA, 1995).

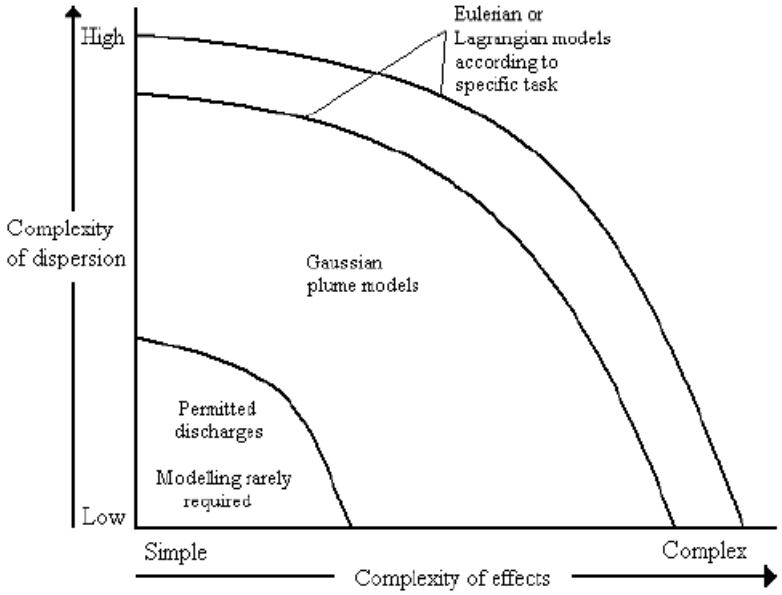

Figure 3.3 The model that can be applied depending on the complexity of the task (Bluett et al., 2004)

Today, several simple mathematical algorithms are used to model pollutant dispersion: the box model, Gaussian model, Eulerian model, and Lagrangian model.

3.2.1 Box Models

The box model is the most basic of the all modelling techniques. This model considered the homogeneous mixture of the pollutant and the average uniform concentration is calculated. The conservation of mass is the basis of box models. The site is seen as a box into which contaminants are released and chemical and physical processes take place. It needs basic meteorology and pollution input, as well as the flow of contaminants into and out of the box (Lettau, 1970; Holmes & Morawska, 2006).

3.2.2 Gaussian Plume Model

The widely used and most popular mathematical models for atmospheric dispersion, Gaussian models, considered the normal statistical distribution of pollutants dispersion under steady state conditions. It is used to determine the distribution from a point source by assuming that the pollutants are distributed

according to the Gaussian distribution (Holmes & Morawska, 2006; Pasquill, 1971; Kakosimos et al., 2011). Detailed Gaussian modelling will be explained in detail in Section 4.5.

3.2.3 Eulerian Model

Eulerian models solve the conservation of continuity momentum and mass equation for a chosen pollutant. Various approximations of the turbulent characteristics of the flow are used, such as k– ε, k– ω, RNG, LES (Holmes & Morawska, 2006; Kakosimos et al., 2011).

3.2.4 Lagrangian Model

Lagrangian models are similar to box models and can be considered as a comprehensive box model. Concentration differences caused by the density differences of the gases, turbulence and molecular diffusion in the box are taken into consideration. A region of air described as a box and the pollutant distribution is calculated according to a reference grid by entering the initial pollutant concentration (Holmes & Morawska, 2006; Kakosimos et al., 2011).

4
MATERIALS AND METHODS

In this study, which aims to model the emission dispersion of the Biga-İçdaş thermal power plant in the Biga district of Çanakkale, details on the general characteristics of the study region, source stacks, meteorology station and air quality monitoring station were given in the first place. Then AERMOD, WRF and CFD models used in the study were explained.

4.1 General Characteristics of The Study Region

Çanakkale province is in the Marmara Region with 9.817 km^2 total area. It consists of two peninsulas and 12 districts including Ayvacık, Bayramiç, Biga, Bozcaada, Çan, Eceabat, Ezine, Gelibolu, Gökçeada, Lapseki, Center, Yenice. The province is located 40°08' north latitudes and 26°24'east longitudes.

In terms of total population, Biga is the largest district of Çanakkale. It is located on the Biga peninsula of Çanakkale province, 90 km from the center. It is surrounded to the east by Gönen, to the west by Lapseki, to the south by Çan and to the north by the Marmara Sea. The population of the district is 90,418 as of 2020 (TUIK, 2020). Biga district where the study area is located is marked on the map in Figure 4.1.

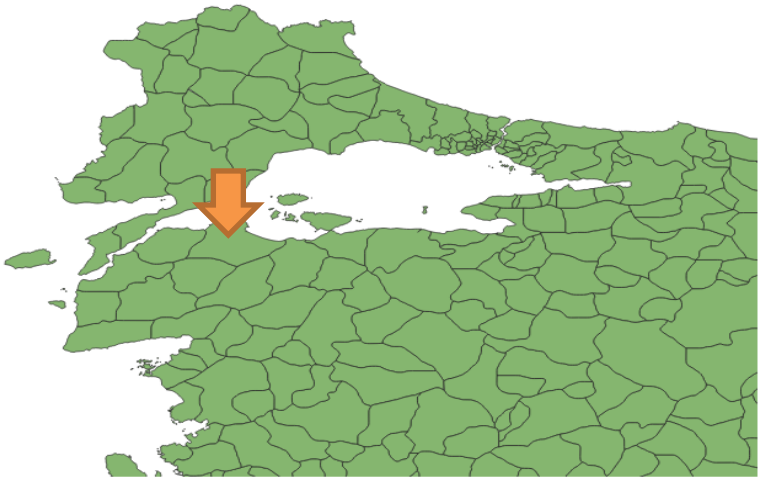

Figure 4.1 The study area location

There are lots of companies producing in different industrial branches in Çanakkale and the industrial operations are mainly carried out the inner areas of the city. The production areas of these companies are primarily food, furniture, wood, manufactured metal, energy and mining.

In Çanakkale, the climate is more close to that of the Mediterranean climate. Summers are hot and dry, while winters are warm and rainy. The climate is almost the same in the province's coastal districts and islands. The altitude from the sea rises in the inner regions and the average temperature is also lower compared to the coastal regions. Depending on the climate characteristics, most of the lands of Çanakkale are covered with forests, mountains and hills. Windy days are encountered in virtually every district much of the year. Depending on seasonal changes the prevailing wind direction of Çanakkale is North-northeast (NNE) and Northeast (NE), respectively (Suerdem & Yildirim, 2009; Akyuz & Kaynak, 2019).

4.2 Source Stacks

The Biga-İçdaş thermal power plant is located in Biga district of Çanakkale. It is operated by İCDAS Steel Energy Shipyard and Transportation Industry Inc. It has an installed capacity of 405 MW with 3 units. It is Çanakkale's third largest power plant. The plant is also the 6th largest imported coal thermal power plant in Turkey. With an average of 2,853,776,454 kilowatt-hours of electricity generation, the Biga Thermal Power Plant provide all electrical energy requirements of 785,731 people in everyday life such as housing, industry, subway transport, lighting (Içdaş, 2013). The detailed Biga-İçdaş thermal power plant stack properties was given in Table 4.1.

Table 4.1 Biga-İçdaş thermal power plant stack properties

Stack Number	Stack Diameter (m)	Stack Height (m)	Exit Temperature (K)	SO_2 Emission rate (kg/h)	PM10 Emission rate (kg/h)	Stack Exit Velocity (m/s)
1	7	150	363	100	15	15.3
2	4	150	403	202	30	33

The plant has two source stacks with 7 and 4 m diameters. Both stacks have 150 m height. They have 15.3 and 33 m/s exit velocity and their SO_2 emission rates are 100 and 202 kg/h, respectively. The data was obtained from Akyuz & Kaynak, 2017.

4.3 Air Quality Monitoring Station (AQMS)

There is an air quality monitoring station in the study region, named Biga-İçdaş. The station is located 40°25'02"N latitudes 27°06'26"E longitudes and it is 3.5 km away from the Biga-İçdaş thermal power plant source stacks. SO_2, PM10, NO, NO_2, NO_X, CO pollutant concentrations are measured hourly and the results are recorded in this station. Biga-İçdaş meteorology station was shown with blue color in Figure 4.2. Air quality is determined as good, medium, bad, dangerous etc. according to the concentrations of pollutants in the ambient air with the classification system called Air Quality Index (AQI), which is widely used all over the world and the results are shared with the public. The measurement results of the past years can be obtained from the website of the National Air Quality Monitoring Network.

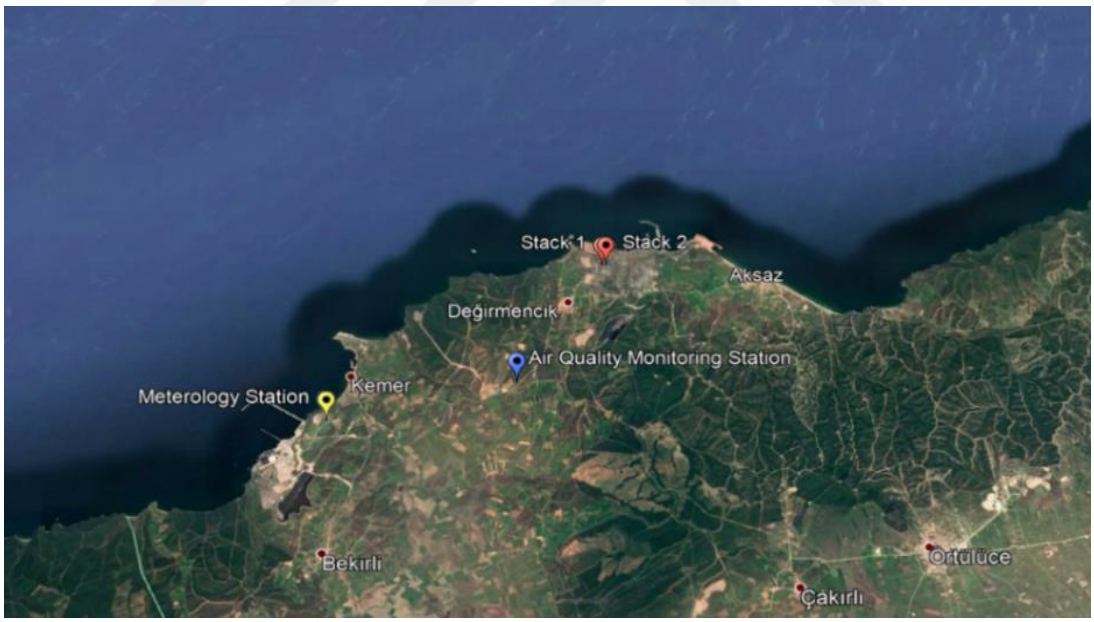

Figure 4.2 Biga-İçdaş thermal power plant source stacks, AQMS, meteorology station

For the year 2014, daily observed SO_2 concentrations at Biga-İçdaş AQMS was shown in Figure 4.3. The data was taken from the National Air Quality Monitoring Network (NAQMN).

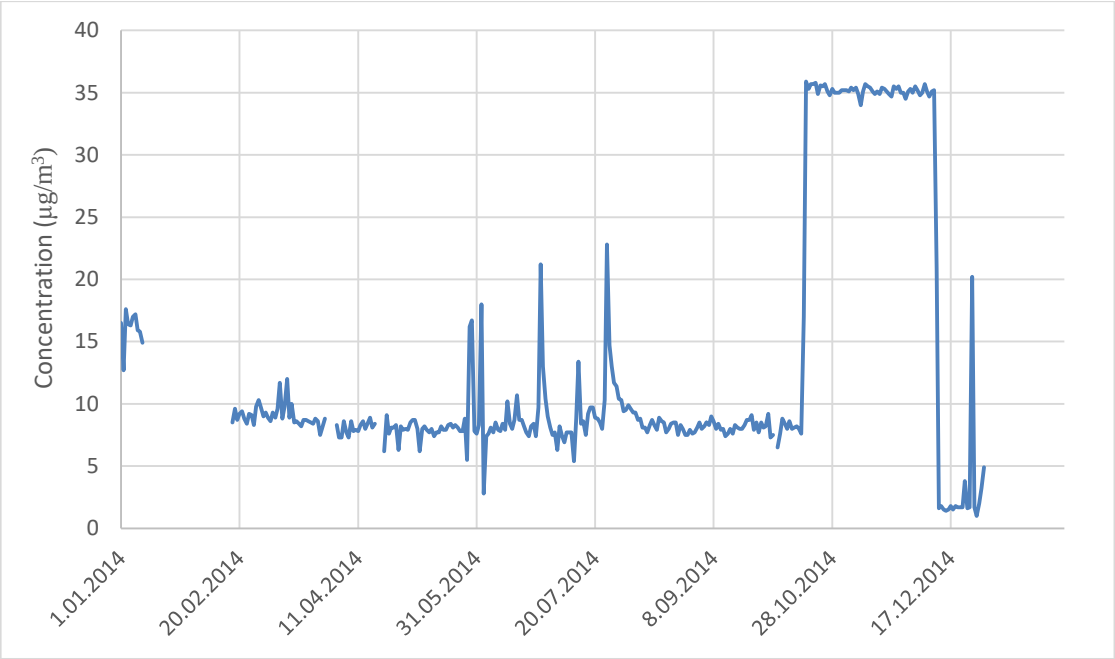

Figure 4.3 Biga-İçdaş AQMS daily observed SO_2 concentrations (µg/m^3)

There was a missing data between January 11, 2014 and February, 16 2014. While the average value for the year 2014 was 13.2 µg/m^3, the highest value was observed as 35.9 µg/m^3 on 17 October.

4.4 Meteorology Station

Biga-Kemer Köyü ground level meteorology station (ID Number: 17614) is available in the study region which is 7 km away from the Biga-İçdaş thermal power plant source stacks. The meteorology station is located 40°24'31.7"N latitudes 27°03'36.0"E longitudes. The station was shown with yellow color in Figure 4.2. For the year 2014, daily observed temperature results was given in Figure 4.4. The data was obtained from General Directorate of Meteorology. Observed daily temperature data was missing between October 22, 2014 and 1 December, 2014. The temperature annual average was 289.04 K for the year 2014 at the meteorology station. The wind rose diagram was created using R openair package and given in Figure 4.5. The annual average value of wind speed was 2.63 m/s. It was varied from 0 to 13.6 m/s. According to the results, SE, NE, NNE were the prevailing wind directions, respectively.

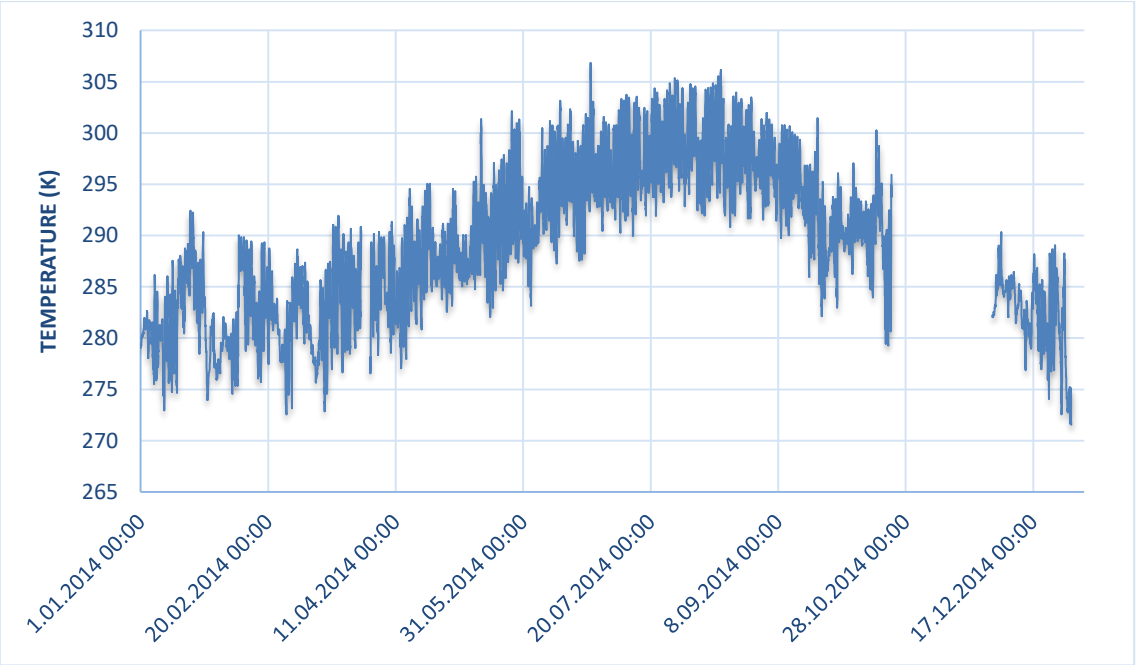

Figure 4.4 Daily observed temperature results at Biga-Kemer Köyü ground level meteorology station for the year 2014

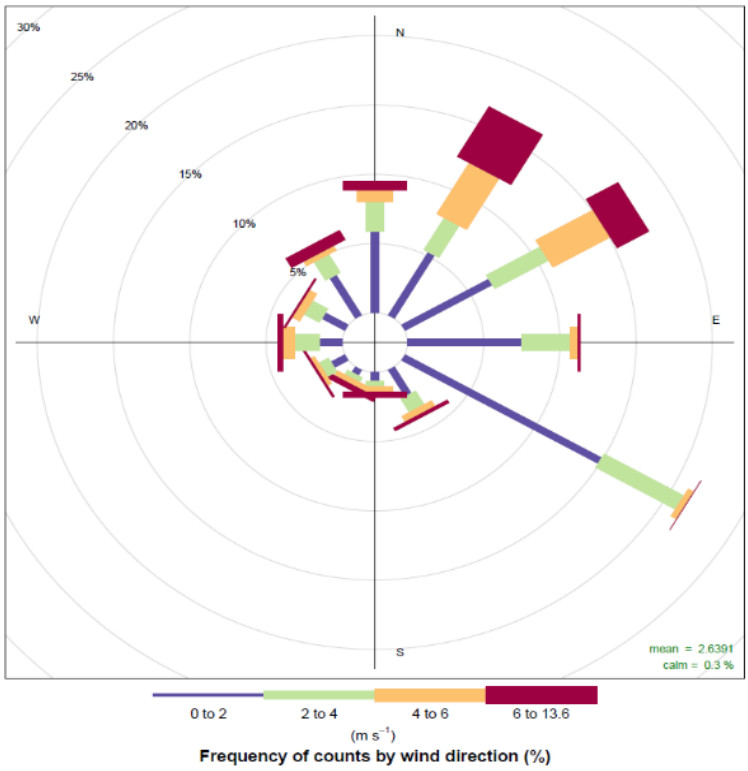

Figure 4.5 Wind rose diagram at Biga-Kemer Köyü ground level meteorology station for the year 2014

4.5 AERMOD

AERMOD is a USEPA's (United States Environmental Protection Agency) recommended steady state plume dispersion model and commonly used for regulatory purposes. It is effective at short distances (<50 km radius) and can successfully be applied to different kinds of terrains. The general behavior of the pollutant gas released into the atmosphere from any source in the atmospheric environment can be mathematically expressed with the Gaussian dispersion model. With the effect of the wind and the Gauss dispersion mechanism, the distribution of the pollutant from a single point source is shown in Figure 4.6. The model determines the horizontal (y) and vertical (z) movement of the plume and calculates the maximum ground-level concentration of the pollutant from a specific point source at a certain distance. The plume released into the atmosphere from a stack height H at a constant rate, then it rises with the effect of momentum and buoyancy force and spreads as it travels in the x direction.

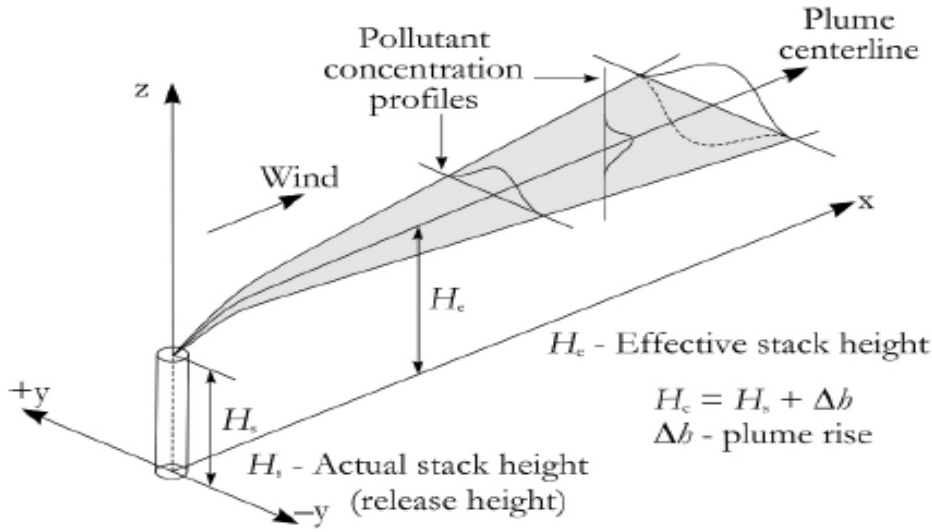

Figure 4.6 The schematic of Gauss dispersion model refers to a single point source (Leelőssy et al., 2014)

The AERMOD model based on steady state Gaussian dispersion equation for point sources. Gaussian distribution equation is given below;

$$C(x,y,z,H) = \frac{Q}{2\pi u\sigma_y\sigma_z}\left[exp\left(\frac{-y^2}{2{\sigma_y}^2}\right)\right]\left\{exp\left(\frac{-(z-H)^2}{2{\sigma_z}^2}\right) + exp\left(\frac{-(z+H)^2}{2{\sigma_z}^2}\right)\right\} \quad (4.1)$$

where C (x,y,z,H) is the concentration of pollutant at the receiving point, H is the effective stack height (m), C is the pollutant concentration (μg/m^3), u is the average wind speed in the x-direction (m/s), Q is the pollutant emission rate (μg/s), σ_y is the standard deviation of the beam in y direction (m), σ_z is the standard deviation of the beam in z direction (m).

The AERMOD model consists of 5 sections in total where the control, source, receptor, meteorological and output options are defined. In control section, pollutants, calculation period, deposition and land use options are specified. The source section includes the location information of the pollutant sources, the parameter information for each pollutant source and the information on how to group the sources. In the receptor section, the grid system where the pollutants will be deposited is defined. In meteorology section, atmospheric conditions are provided for the model area through the meteorological preprocessor of AERMOD, named AERMET. In output section, the format of the output results are determined.

4.5.1 Model Domain and Topography

In the AERMOD model domain, Cartesian grid was used with 250 m grid spacing, the total model domain was 25 km × 25 km. The selected model domain topography was shown in Figure 4.7.

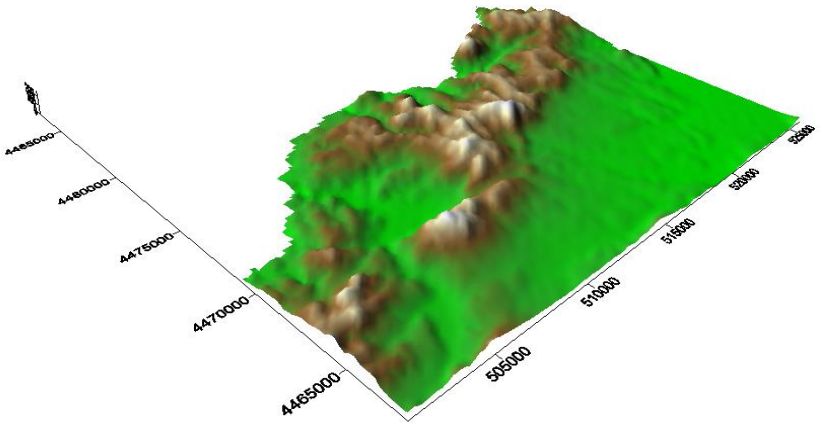

Figure 4.7 AERMOD model domain topography

For the topography 30 meter SRTM (The Shuttle Radar Topography Mission) data was used and UTM (Universal Transverse Mercator) zone 42 was selected for the study area. The data was downloaded from US Geological Survey's EROS Data Center available at www.usgs.gov. Visualization was done with the help of Surfer program.

4.5.2 AERMET Preprocessor

AERMOD model needs surface meteorology data in *.sfc file format and profile meteorology data in *.pfl file format which are created by AERMET, the meteorological preprocessor of the AERMOD model, by processing the surface and upper air data. Data processing procedure of AERMET preprocessor was given in Figure 4.8.

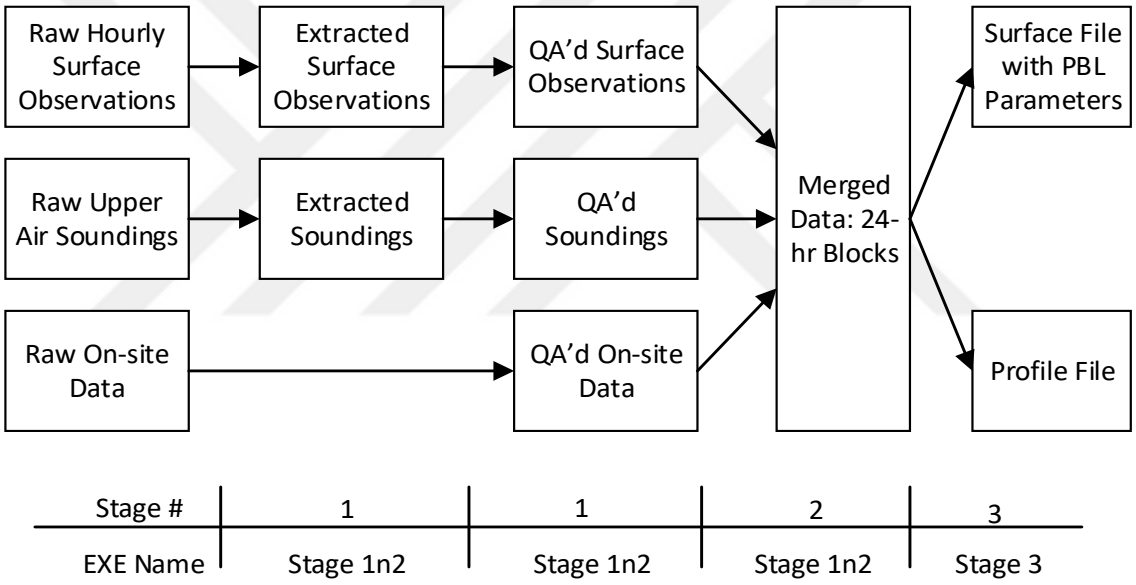

Figure 4.8 AERMET data processing procedure (U.S. EPA, 2004)

In the first step, the hourly data of the raw surface and upper atmosphere are checked for quality and the mixing height is calculated. In the second step, the data are combined into a single file. In the third step, hourly PBL values are calculated by defining the land use parameters which are surface roughness, albedo and bowen ratio. Finally, profile file (*.pfl) containing wind speed, wind direction, temperature and standard deviation of wind components at different levels and surface meteorology file (*.sfc) containing surface meteorology data are prepared.

In this study, the required surface meteorological data (temperature, wind speed, and wind direction) for the AERMET preprocessor was obtained from the Biga-Kemer Köyü station. The station had 5 weeks of missing temperature data between 22, October 2014 and 30, November 2014. The missing data was completed with the Weather Research and Forecasting (WRF) model which will be described in Section 4.6. Also there is no cloud cover data at meteorology station. When all the cloud cover is missing, AERMET can produce *.sfc and *.pfl files with missing value 99, but AERMOD cannot produce concentration results. Therefore, we used the WRF model to extract the missing cloud cover data and used as input to the AERMET preprocessor. For the upper air data (atmospheric pressure, temperature, dew point temperature, wind direction and wind speed at different altitudes) Istanbul radiosonde station was used which is the closest station with a distance of 180 km to the study region. The upper air data can be downloaded from https://ruc.noaa.gov/raobs/ in fsl format. As a function of land use and seasons different values are used for albedo, bowen ratio and surface roughness (m). Table 4.2 shows the land use parameters used in the preprocessor of AERMET.

Table 4.2 The land use parameters used in the preprocessor of AERMET

Parameter	Range (Water)	Range (Urban)
Albedo	0.10 - 0.2	0.14 - 0.35
Bowen Ratio	0.1	0.5 - 1
Surface Roughness (m)	0.001	1

The *.sfc and *.pfl files generated by the AERMET preprocessor were used as input to the AERMOD model. The two source stacks are defined as “point source” and the AQMS defined as “receptor point” in the model. The year 2014 was chosen as the calculation year in order to compare with previous studies in the same region using different models. Then the model was run to obtain hourly maximum, daily maximum, and annual ground level SO_2 concentration values.

4.6 Weather Research and Forecasting Model (WRF)

The 5 weeks of missing temperature data at the Biga-Kemer Köyü meteorology station was completed with The Weather Research and Forecasting (WRF) Model. It is an open source numerical weather prediction model developed at NCAR (National Center for Atmospheric Research) and commonly used by researchers for forecasting and analysis purposes. The model can be operated in 2 different ways as NMM (Non-hydrostatic Mesoscale Model) and ARW (Advanced Research WRF). In this study WRF-ARW 4.0.3 version was used. The flow chart of the model consists of external data source, WRF Pre-Processing System (WPS), WRF Model and Post-Processing & Visualization (Figure 4.9).

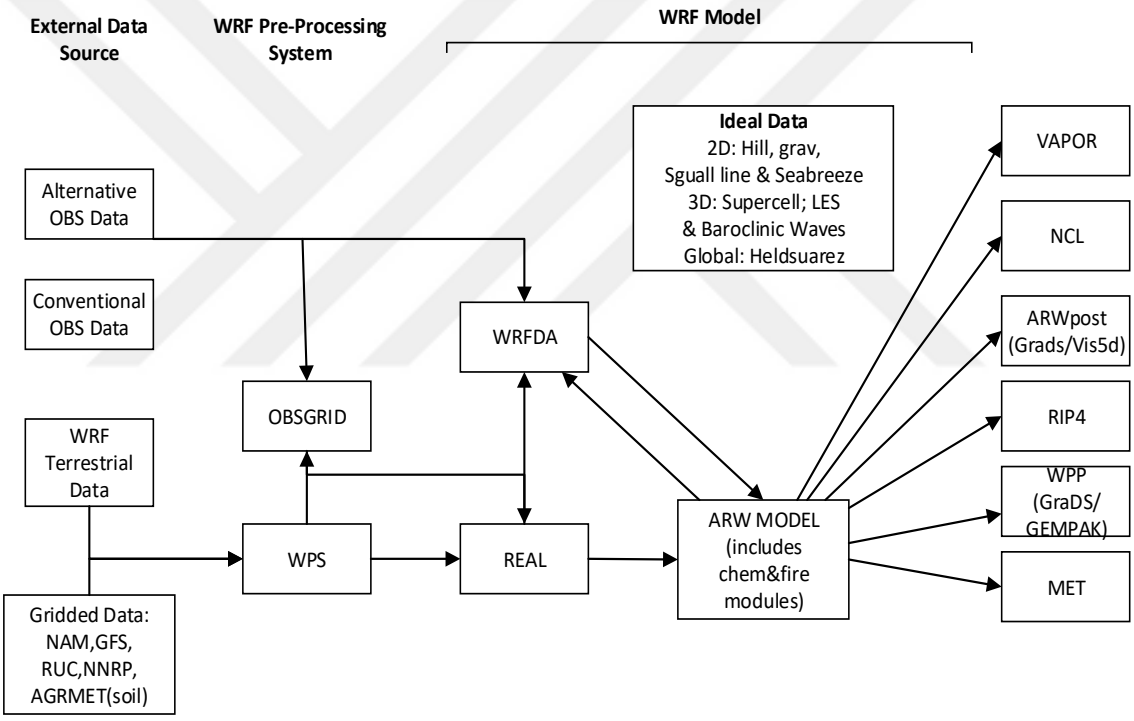

Figure 4.9 Weather Research and Forecasting (WRF) model flow chart

WPS (WRF Preprocessing System) is the main component of WRF Model. It determines the grid for the WRF model and generates map, elevation and land data. WPS matches meteorological data with terrain data in 3 steps: geogrid, ungrib and metgrid (Figure 4.10). The namelist.wps file is edited to implement the experimental design which was given in Appendix A. In geogrid step, the model domain is defined and the terrain data is interpolated to the grid points of the model. For each domain geo_ em netcdf files were created. In ungrib step, GFS files

in grib2 format is converted to appropriate data format of the WRF model. In metgrid step, the meteorological fields extracted by ungrib are interpolated to the simulation domain defined by geogrid and met_em files are built for real.exe. The model parameters are configured by namelist.input file (Appendix B). Real.exe interpolates met_em files to the chosen number of model vertical levels to generate wrfbdy and wrfinput netcdf files for wrf.exe. Then the meteorological model was run.

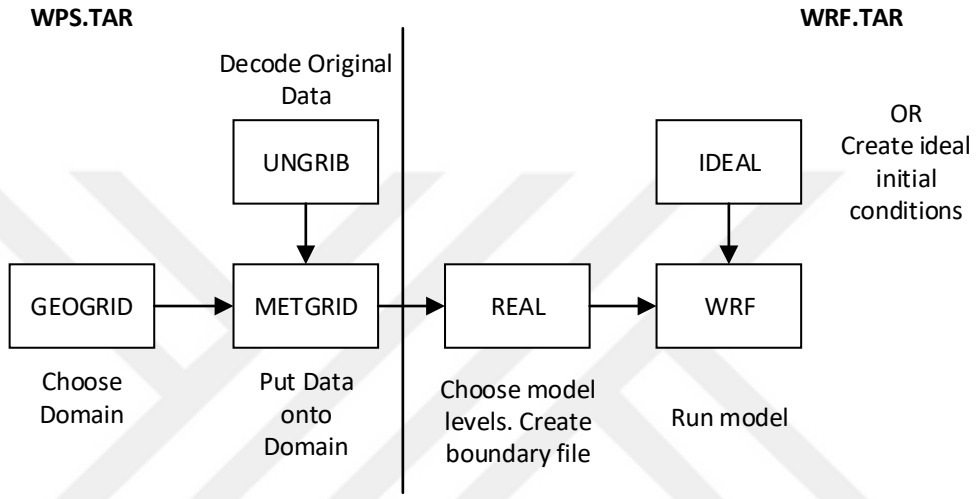

Figure 4.10 WPS and WRF Flow

4.6.1 WRF Model Setup

The WRF model domain consists of two nested domains with 10 km resolution outer domain and 3.3 km resolution inner domain. They have 29 and 25 grid points respectively. Figure 4.11 shows the model area boundaries. To provide initial and boundary conditions for the model, the National Centers for Environmental Prediction's (NCEP) Global Forecast System 6 hour (GFS-ANL) analysis dataset was used. The model run for one year between 1st January, 2014 00UTC-1st January, 2015 00UTC. Various tests were done to obtain the best parameterization. Table 4.3 shows the physical parameterizations used in the WRF simulation. It includes WSM 5- class scheme for Microphysics, Kain-Fritsch (new Eta) scheme for Cumulus Parameterization (Kain, 2004), The Yonsei University (YSU) scheme for Planetary Boundary Layer (PBL), Noah-MP land-surface model for Land-Surface (Dudhia, 2001), MM5 Monin-Obukhov scheme for Surface Layer

Physics, RRTM for Longwave Radiation Scheme (Mlawer et al., 1997), Dudhia for Shortwave Radiation Scheme (Dudhia, 1989).

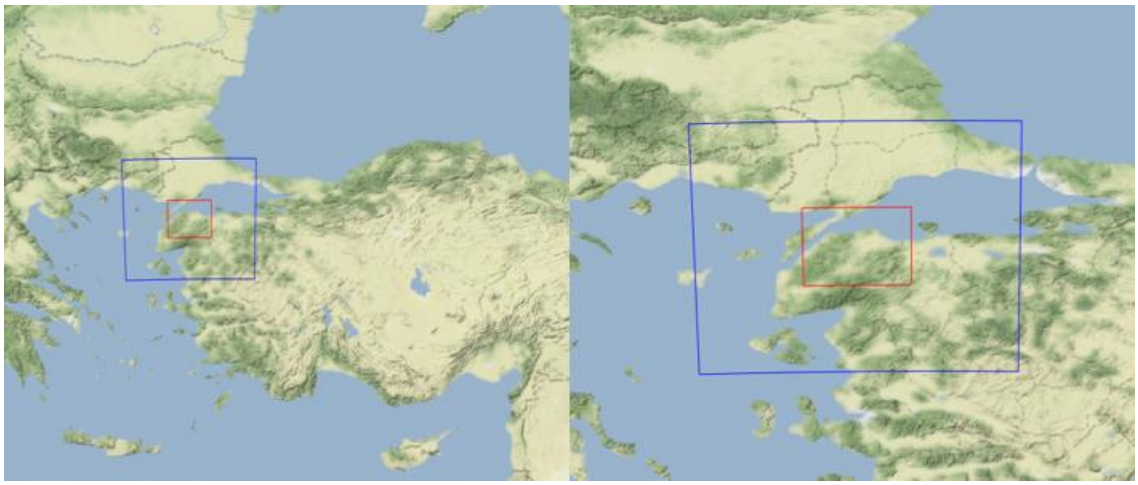

Figure 4.11 WRF Model outer (blue line) and inner (red line) area boundaries

Table 4.3 Physical Parameterizations used in WRF Model

Physics	
Microphysics Scheme	WSM 5- class scheme
Cumulus Parameterization Scheme	Kain-Fritsch (new Eta) scheme
Planetary Boundary Layer (PBL) Scheme	The Yonsei University (YSU) scheme
Land-Surface Model	Noah-MP land-surface model
Surface Layer Physics	MM5 Monin-Obukhov scheme
Longwave Radiation Scheme	RRTM
Shortwave Radiation Scheme	Dudhia

4.7 WRF Model Results Verification Methodology

Verification is the process of determining the accuracy of the predictions by comparing them with the observations results. Various verification techniques are available in the literature including the mean bias (MB), coefficient of correlation (r) and root mean square error (RMSE), fractional bias (FB), Index of Agreement (IOA). In this study the root mean square error (RMSE), the mean bias error (MBE) and R-squared (R^2) was used for verification of the WRF model temperature results.

RMSE is the standard deviation of the estimation errors. The RMSE values range from 0 to ∞. The lower RMSE values (close to 0) indicates better model

performance. R^2 is the coefficient of determination and ranges from 0 to 1. The lower RMSE values (close to 0) indicates better model performance, whereas the higher R^2 values (close to 1) shows that the regression line matches the data well and the performance of the model is better. The direction of the error bias is defined by MBE. When predictions are lower in value than observations, a negative MBE occurs. The mean bias error (MBE), the root mean square error (RMSE) are based on the term (P_i-O_i). They calculated according to (Willmott, 1982) where N is the number of data, P is the predicted data, O is the observed data. Verification study was carried out on the daily average value for temperature and MBE, RMSE and R^2 were calculated from the following equations.

$$MBE = N^{-1} \sum_{i=1}^{N} (P_i - O_i) \tag{4.2}$$

$$RMSE = \left[N^{-1} \sum_{i=1}^{N} (P_i - O_i)^2 \right]^{0.5} \tag{4.3}$$

$$R^2 = \frac{(\sum_{i=1}^{n} (O_i - O_m)(P_i - P_m))^2}{\sum_{i=1}^{n} (O_i - O_m)^2 \sum_{i=1}^{n} (P_i - P_m)^2} \tag{4.4}$$

4.8 Computational Fluid Dynamics (CFD)

Computational Fluid Dynamics (CFD) is a branch of science that enables the simulation of fluid flow, heat transfer and other related physical phenomena with the help of computers. Although CFD was only used in research in the early 80s, over time it became an important field in engineering and today, the use of CFD has become increasingly important and has many different applications such as electrical engineering, chemical process engineering, environmental engineering, hydrology, aerospace, automotive and meteorology. The steps for solving a CFD problem are: pre-processing, solve, post processing (Figure 4.12). At preprocessing step, the geometry definition, geometry discretization, boundary conditions definition and physical model definition were made. Different programs, such as SpaceClaim, AutoCad, Rhino, and SketchUp, can be used to create geometry. The mesh was created by specifying the input and output points. At solve step, the

solution was computed using Navier-Stokes equations. At last step, Post-processing was done with streamline or contour plots.

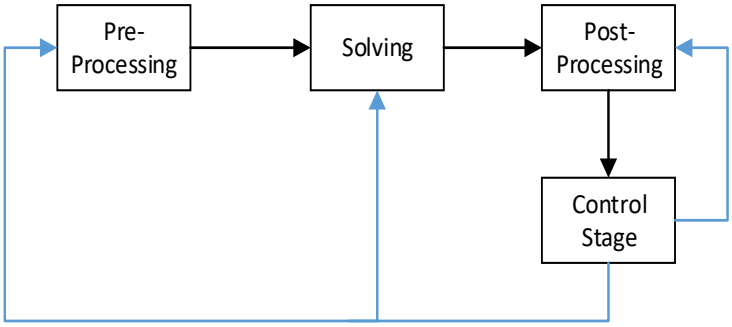

Figure 4.12 CFD process steps

Navier-Stokes equation is the basis of CFD mechanism that consist of conservation of mass, momentum and energy. We can derive the equations as follows;

Continuity Equation

$$\frac{D_\rho}{Dt} + \rho \frac{\partial U_i}{\partial x_i} = 0 \tag{4.5}$$

Momentum Equation

$$\underbrace{\rho \frac{\partial U_j}{\partial t}}_{\text{I}} + \underbrace{\rho U_i \frac{\partial U_j}{\partial x_i}}_{\text{II}} = \underbrace{-\frac{\partial P}{\partial x_j}}_{\text{III}} \underbrace{-\frac{\partial \tau_{ij}}{\partial x_i}}_{\text{IV}} + \underbrace{\rho g_j}_{\text{V}} \tag{4.6}$$

I: Local change with time

II: Momentum convection

III: Surface force

IV: Molecular-dependent momentum exchange (diffusion)

V: Mass force

Energy Equation

$$\underbrace{\rho c_\mu \frac{\partial T}{\partial t}}_{\text{I}} + \underbrace{\rho c_\mu U_i \frac{\partial T}{\partial x_i}}_{\text{II}} = \underbrace{-P \frac{\partial U_i}{\partial x_i}}_{\text{III}} + \underbrace{\lambda \frac{\partial^2 T}{\partial {x_i}^2}}_{\text{IV}} \underbrace{-\tau_{ij} \frac{\partial U_j}{\partial x_i}}_{\text{V}} \tag{4.7}$$

I: Local energy change with time

II: Convective term

III: Pressure work

IV: Heat flux (diffusion)

V: Irreversible transfer of mechanical energy into heat

In this study, the CFD model was implemented using ANSYS R18.2 Fluent solver. SO_2 dispersion pattern was conducted using critical wind speeds and directions obtained from Biga-Kemer Köyü meteorology station under consideration of the topographical features in the study region.

The three-dimensional geometry of the study area was created with the Autodesk InfraWorks Program, by taking the source stacks in one corner and the AQMS in opposite corner (Figure 4.13). The terrain was positioned on the ground in a 3 km x 2.5 km model area, and the height was created using planetary boundary (PBL) heights. The lower part of the atmosphere, known as the PBL, is where the majority of air pollution occurs. More accurate and realistic predictions of pollutant dispersion processes are realized with an accurate atmospheric boundary flow in the computing area. Therefore, we obtained the PBL heights for all cases from the AERMOD simulation results. To obtain a 3D geometry, geometry editing operations were performed in ANSYS SpaceClaim interface.

In this study, firstly, the wind direction blowing directly to AQMS was determined, which is 37^0. It is known that when wind speeds of less than 1 m/s entered the AERMOD model, the concentrations rise to unrealistically high levels at calm conditions (U.S. EPA, 2019). For this reason, the conditions where the wind is greater than 1 m/s are selected for CFD simulations in order to obtain a more accurate comparison between results. We also didn't use PBL values that were lower than the stack height (150 meter) and eliminated the days when observation data at AQMS was unavailable. After all the arrangements were made, seven simulations was conducted for seven different scenarios that the wind was blowing directly to the AQMS. For these cases, wind speed and PBL heights computed using AERMET were shown in Table 4.4.

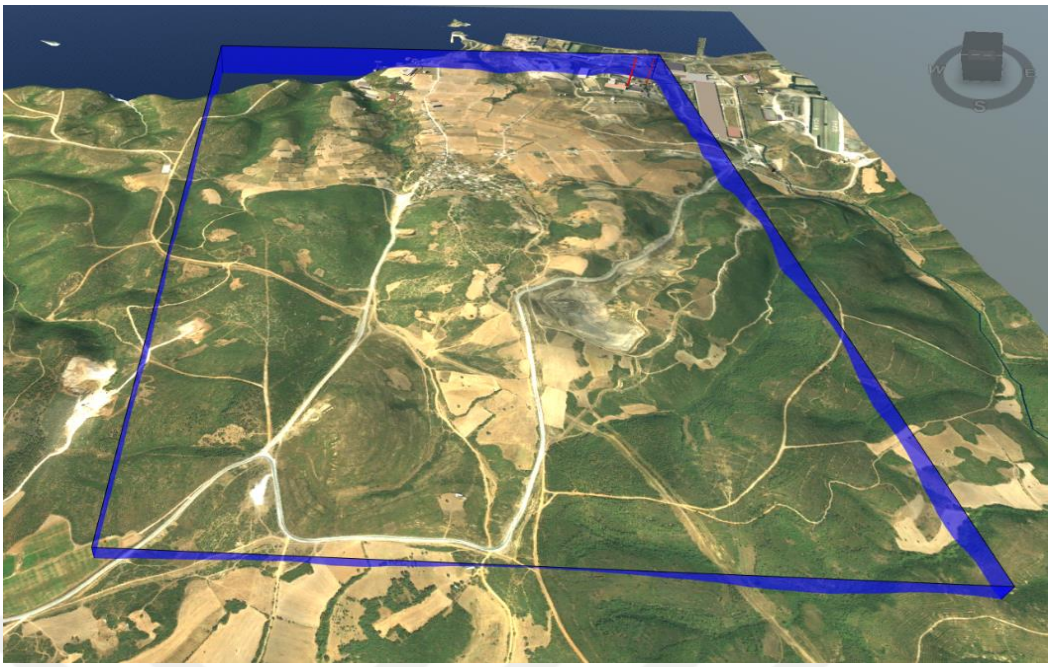

Figure 4.13 Three dimensional geometry of the study area

Table 4.4 The cases used in CFD model simulations

Case Number	Date-Hour	Wind Speed (m/s)	PBL Height (m)
1	08.01.2014-11:00	1.5	392
2	08.01.2014-12:00	1.5	413
3	08.01.2014-13:00	1.5	427
4	13.03.2014-12:00	3.6	663
5	21.03.2014-08:00	5.7	333
6	27.03.2014-09:00	4.1	393
7	27.03.2014-12:00	5.7	616

At the meshing interface, an optimal mesh size was created by considering the stack sources and AQMS locations (Figure 4.14). Two stack inlets, two wind inlets and two pressure outlet points are defined within the model area. By using proximity and curvature advanced size option and quadratic element order, a good

network was obtained that adequately captured all the geometric properties of the terrain. For all cases the mesh had different element number varying between 3,994,849 and 4,028,987. An example of a mesh for case 1 was given in Figure 4.14.

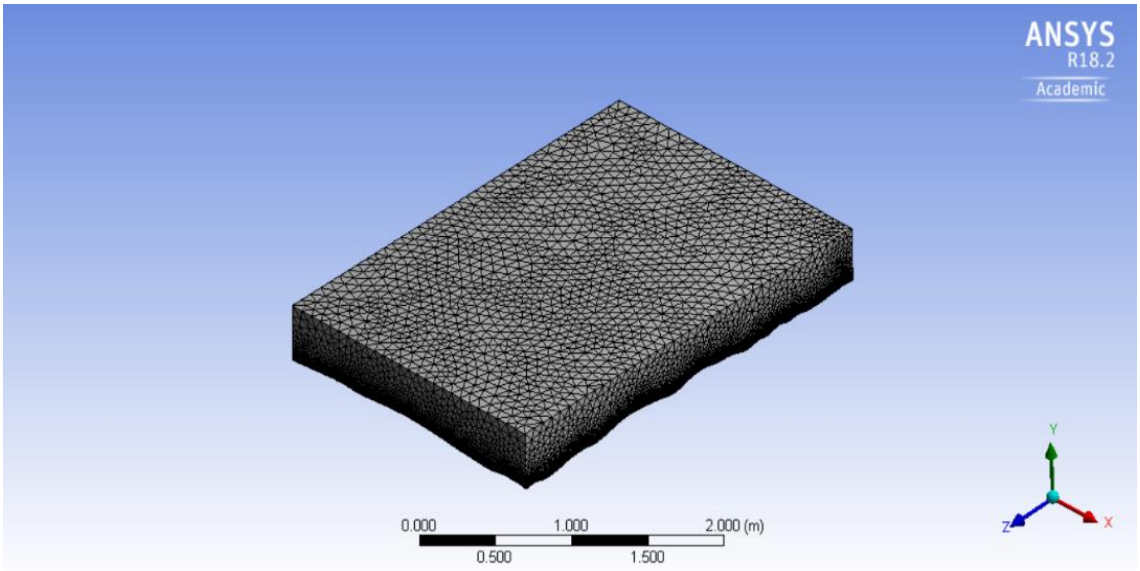

Figure 4.14 The view of the Case 1 three-dimensional terrain on the meshing interface

In the setup part, the analysis are implemented as hybrid initialization using realizable k-ε turbulence model and standard wall functions. And species transport was enabled to investigate the impact of topographical and meteorological factors on pollutant concentration.

The realizable k-ε turbulence model transport equations as follows;

$$\frac{\partial}{\partial t}(\rho\varepsilon) + \frac{\partial}{\partial x_j}(\rho\varepsilon u_j) = \frac{\partial}{\partial x_j}\left[\left(\mu + \frac{\mu_t}{\sigma_\varepsilon}\right)\frac{\partial \varepsilon}{\partial x_j}\right] + \rho C_1 S\varepsilon - \rho C_2 \frac{\varepsilon^2}{k+\sqrt{v\varepsilon}} + C_{1\varepsilon}\frac{\varepsilon}{k}C_{3\varepsilon}G_b + S_\varepsilon \quad (4.8)$$

$$C_1 = max\left[0.43, \frac{\eta}{\eta+5}\right] \quad (4.9)$$

$$\eta = S\frac{k}{\varepsilon} \quad (4.10)$$

k is the turbulence kinetic energy and ε is the turbulence energy dissipation rate, μ_t is the turbulent viscosity, σ_ε is the turbulent Prandtl number for ε, S_ε is the user defined source term, G_b is the generation of turbulence kinetic energy due to buoyancy, $C_{1\varepsilon}$ and C_2 are constants.

For solution, the SIMPLE (Semi-Implicit Method for Pressure-Linked Equations) algorithm was used. For flow and transport equations, the second-order upwind scheme was used. For each case, 1500 iteration was applied to reach 1e-004 converged level.

5
RESULTS AND DISCUSSION

5.1 Weather Research and Forecast (WRF) Model Results

The predicted temperature, wind speed, and wind direction values obtained from the WRF model were compared with the Biga-Kemer Köyü meteorology station observed values. The predicted (WRF) and observed (Biga-Kemer Köyü station) daily temperature values were given in Figure 5.1.

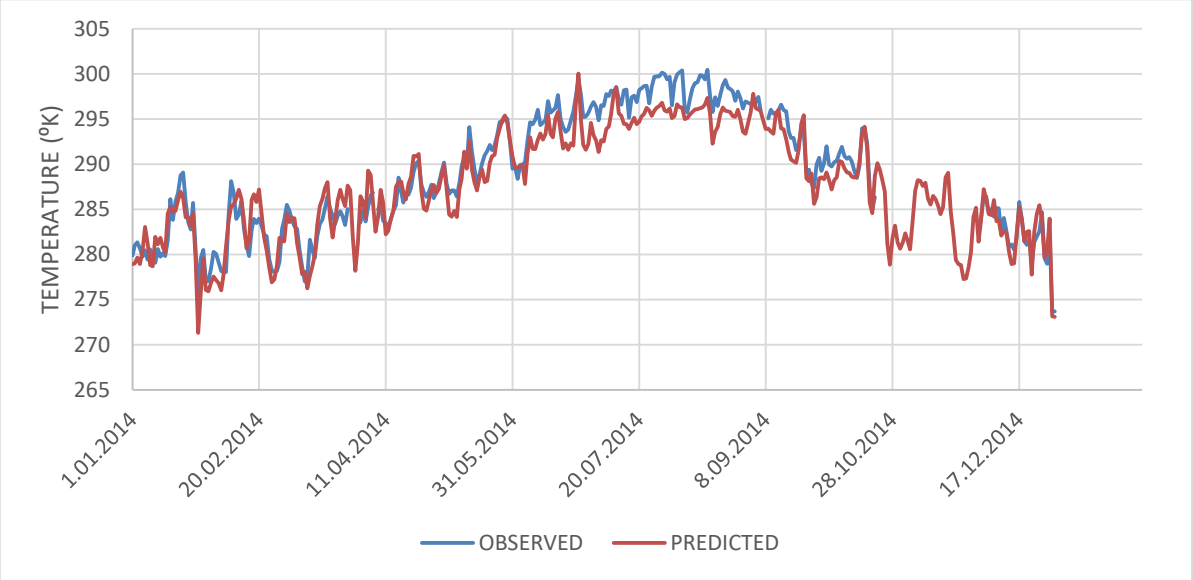

Figure 5.1 The predicted (WRF) and observed (Biga-Kemer Köyü station) daily temperature values

According to the WRF model results the annual average value of the temperature for the year 2014 was found 288.1^{0}K at the meteorology station while the observed value was 289.0^{0}K. The trend line could be followed by the WRF model. When the results are examined, it is seen that the WRF model produces underestimated values for June, July, and August. In AERMOD, the values of convective parameters such as Monin–Obukhov length, the surface friction velocity, and convective velocity scale may be affected by temperature deviations, but in our study, these minor variations were unlikely to have a noticeable impact on the final result. However, in general, the predicted temperature values

demonstrated strong compliance with the values of the Biga-Kemer Köyü meteorology station.

The wind rose diagram was created using the data obtained from the WRF model for the year 2014 using the R openair package (Figure 5.2). The wind speed ranged from 0 to 12.5 m/s with an annual average value of 3.2 m/s and the prevailing wind direction was NE, NNE, SW, according to the results of the WRF simulation.

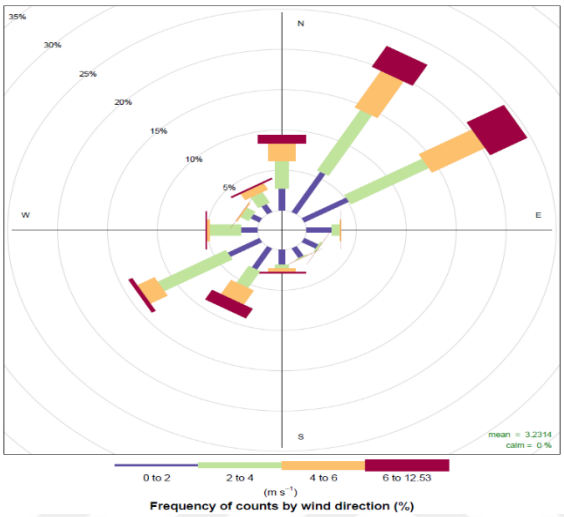

Figure 5.2 The wind rose diagram for the year 2014 obtained from the WRF model

5.1.1 WRF Verification Results

R^2, RMSE, and MBE results obtained from the verification are shown in Table 5.1. R^2, RMSE, and MBE were 0.938, 2.00, and -0.937 respectively. The relation between actual measurement temperature results and the WRF model results for the year 2014 were given in Figure 5.3. It seems that the regression line fits the data well. The negative MBE value shows that the WRF model predicted lower temperature results than the observations. According to the verification results, it can be inferred that WRF has a good performance in predicting temperature values.

Table 5.1 Verification results for the daily average temperature values

	R^2	RMSE	MBE
Temperature	0.938	2.00	-0.937

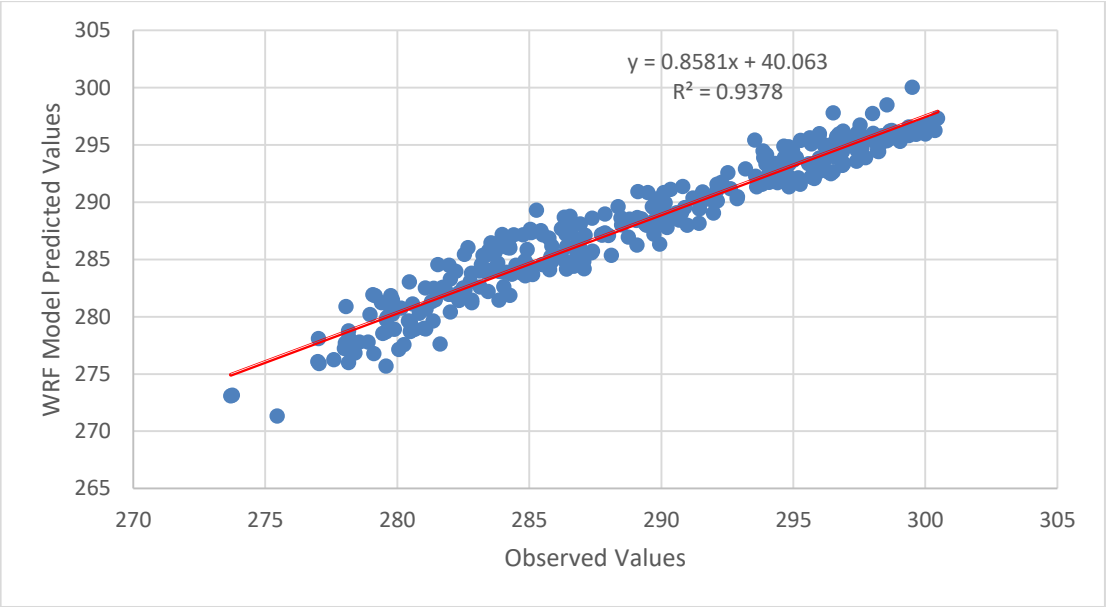

Figure 5.3 The relation between actual measurement temperature results and WRF model results for the year 2014

5.2 AERMOD Model Results

For the year 2014, the annual, daily maximum, and hourly maximum SO_2 concentration values were calculated with the AERMOD model and SO_2 distribution plots over the study area were given in Figure 5.4.

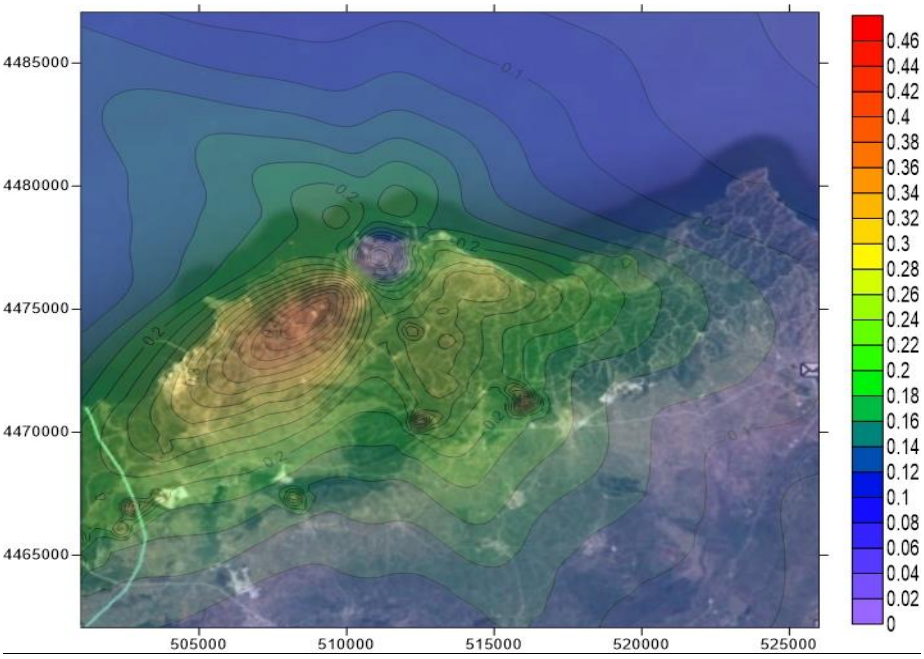

(a)

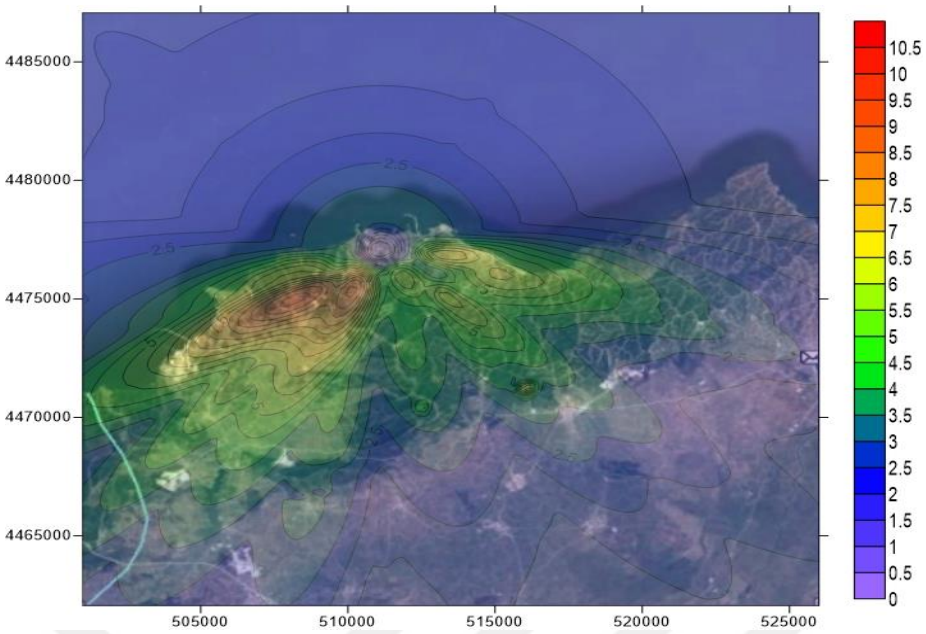

(b)

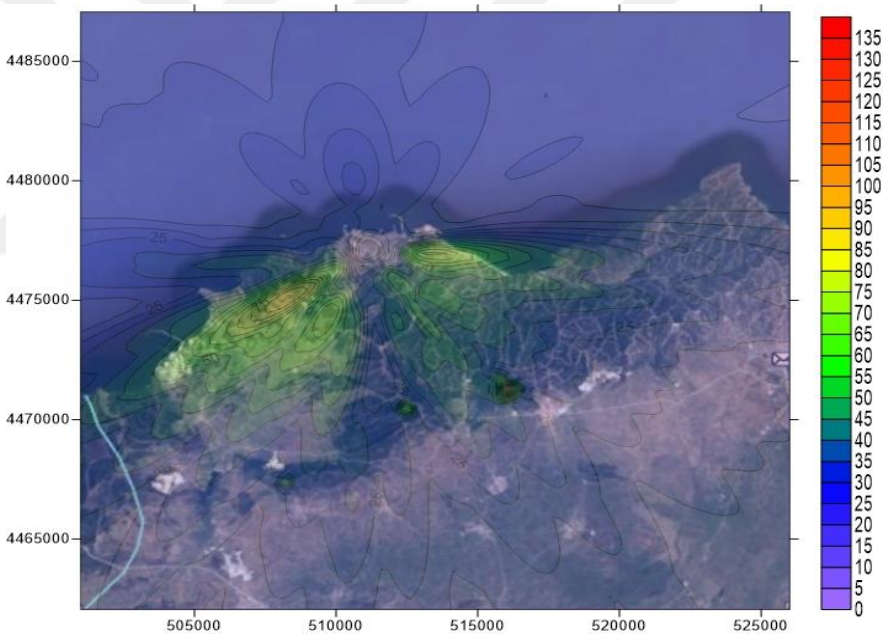

(c)

Figure 5.4 The annual (a) 24-hr maximum (b) and hourly maximum (c) SO_2 concentration (µg/m^3) distribution plots for the year 2014

The annual average maximum concentration was found to be 0.46 µg/m^3 at X: 516,000, Y: 4,471,060 UTM coordinates. At the receptor point, the annual average concentration was calculated as 0.40 µg/m^3. The concentration distribution of the annual average is significant in determining the parts of the region that will be

exposed to long-term exposure. From this point of view, it was seen that the highest SO_2 concentration occurs at 180 m altitudes in the southeast direction of the source stacks. It was approximately 3.25 km from the source. There is no settlement area or agricultural activity in the area. Twenty-four-hr maximum concentration was calculated as 10.22 μg/m^3 at X: 508,250, Y: 4,475,060 UTM coordinates. At receptor, it was found as 7.89 μg/m^3. The highest concentration for hourly value in the region was calculated as 155.22 μg/m^3 at X: 516,000, Y: 4,471,310 UTM coordinate, while it was found as 56.32 μg/m^3 at the receptor point. This value is obtained as the highest possible contamination value under current conditions. The hourly distribution of SO_2 was quite similar to the annual distribution.

5.3 CFD Model Results

The CFD model was run for seven different cases to simulate the dispersion of SO_2 emissions from the stacks of the plant over the study area and iso-surfaces based on SO_2 mass fraction were generated for all cases. The generated iso-surfaces have a unique concentration value. They are shown in Figure 5.5.

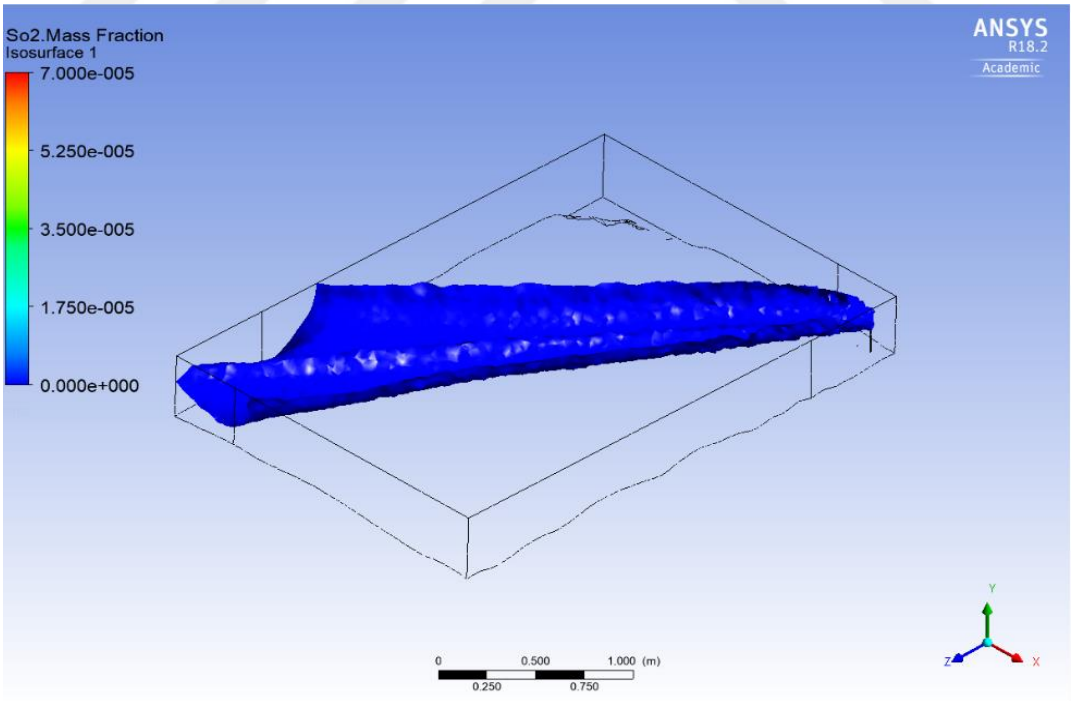

(a) Case 1 – 392 m (PBL height)

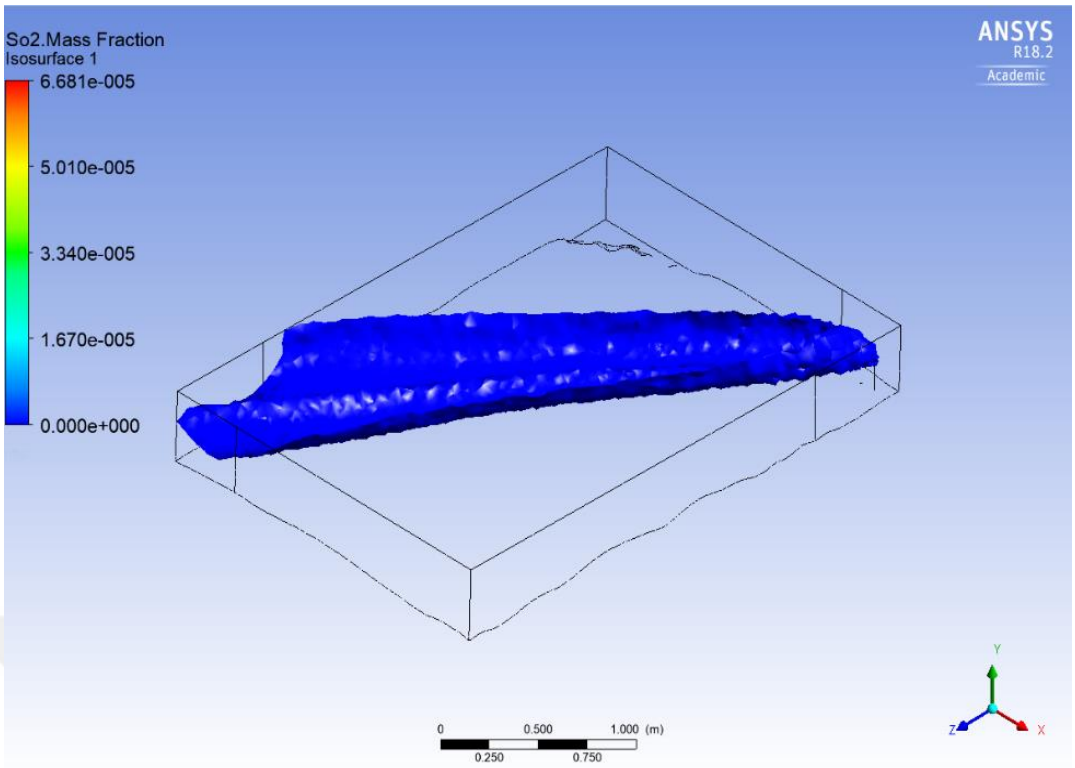

(b) Case 2 – 413 m (PBL height)

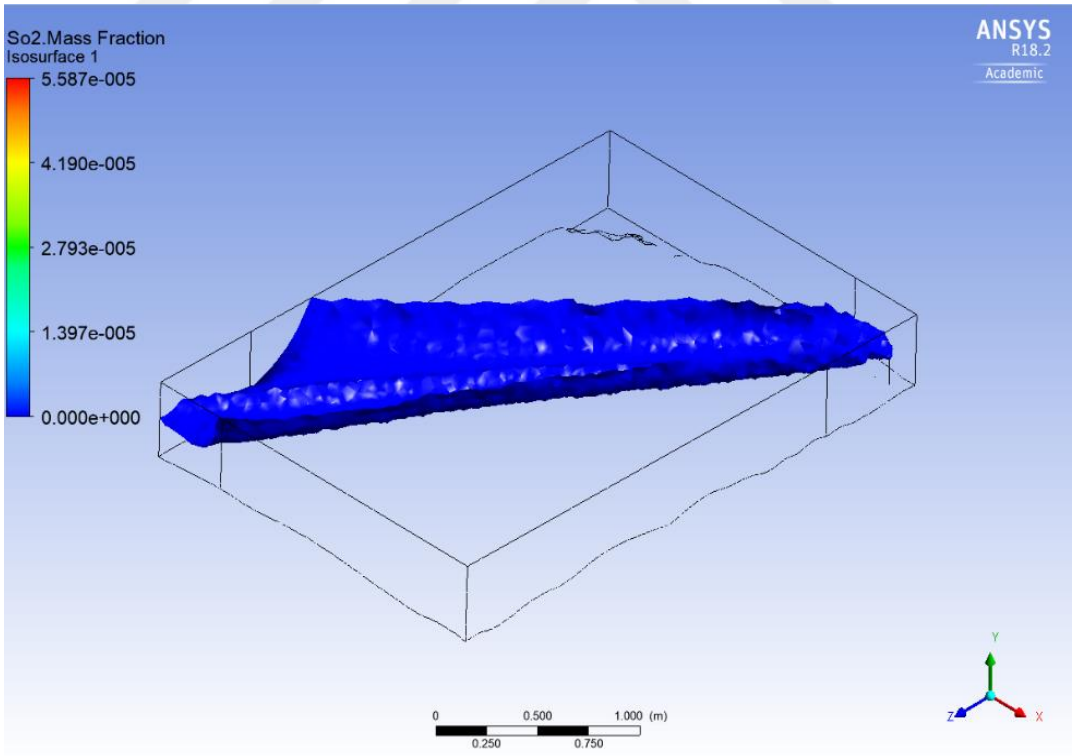

(c) Case 3 – 427 m (PBL height)

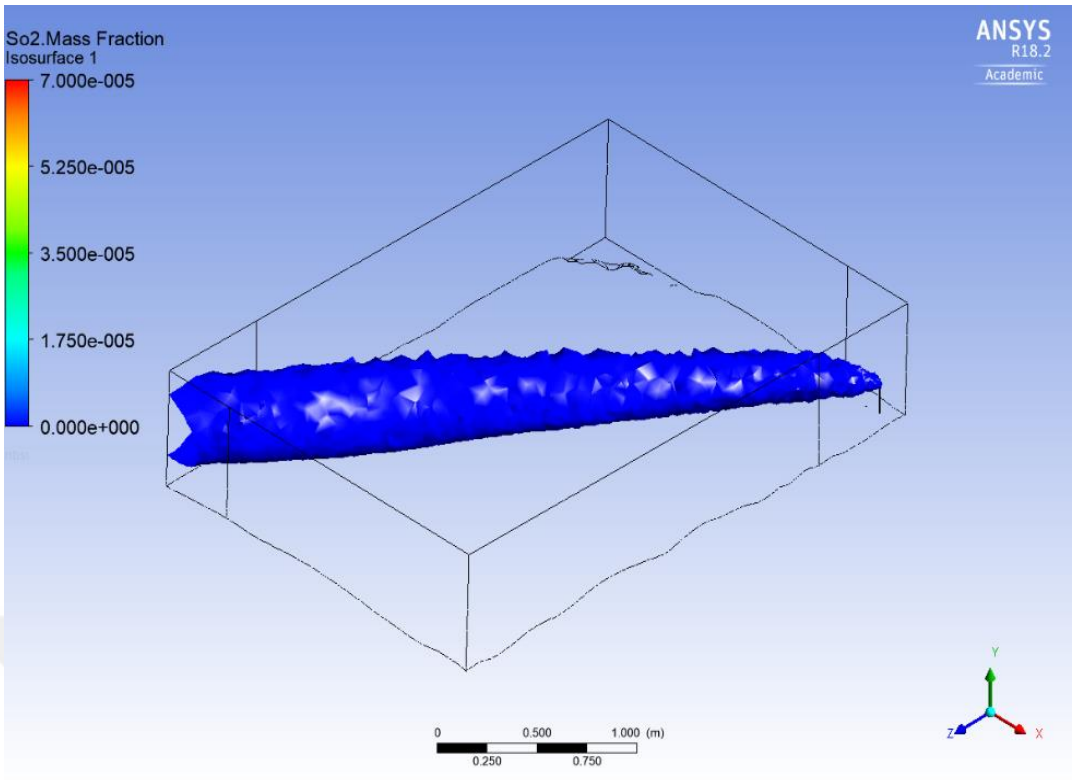

(d) Case 4 – 663 m (PBL height)

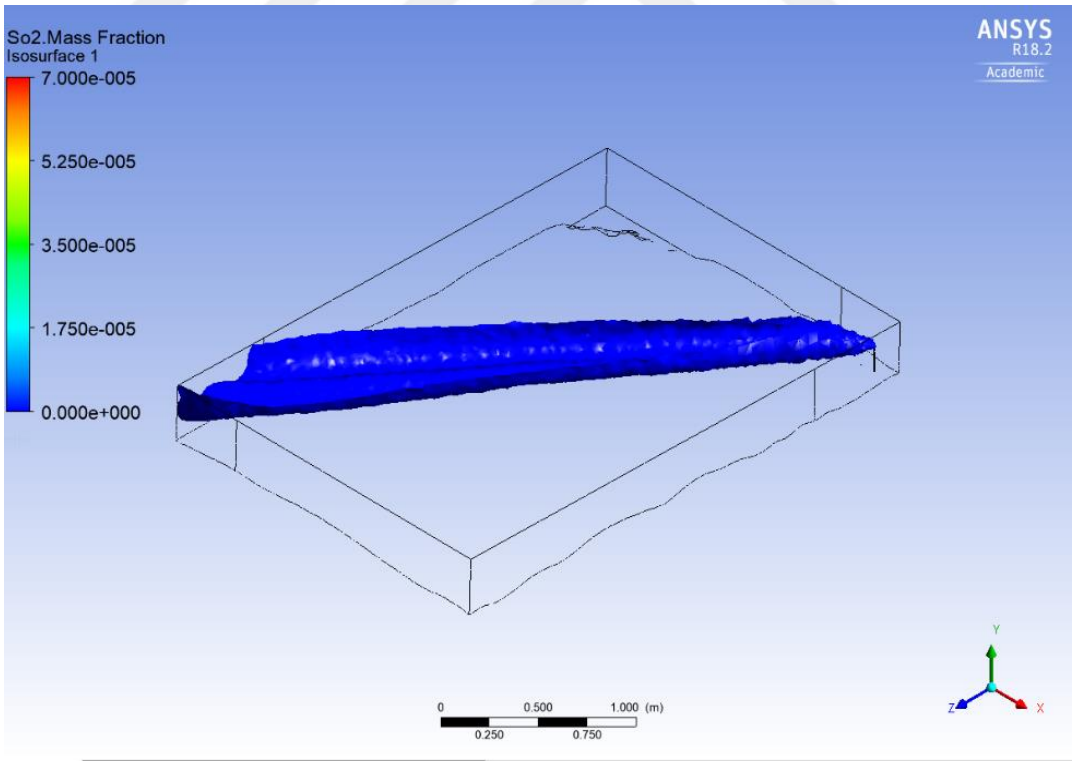

(e) Case 5 – 333 m (PBL height)

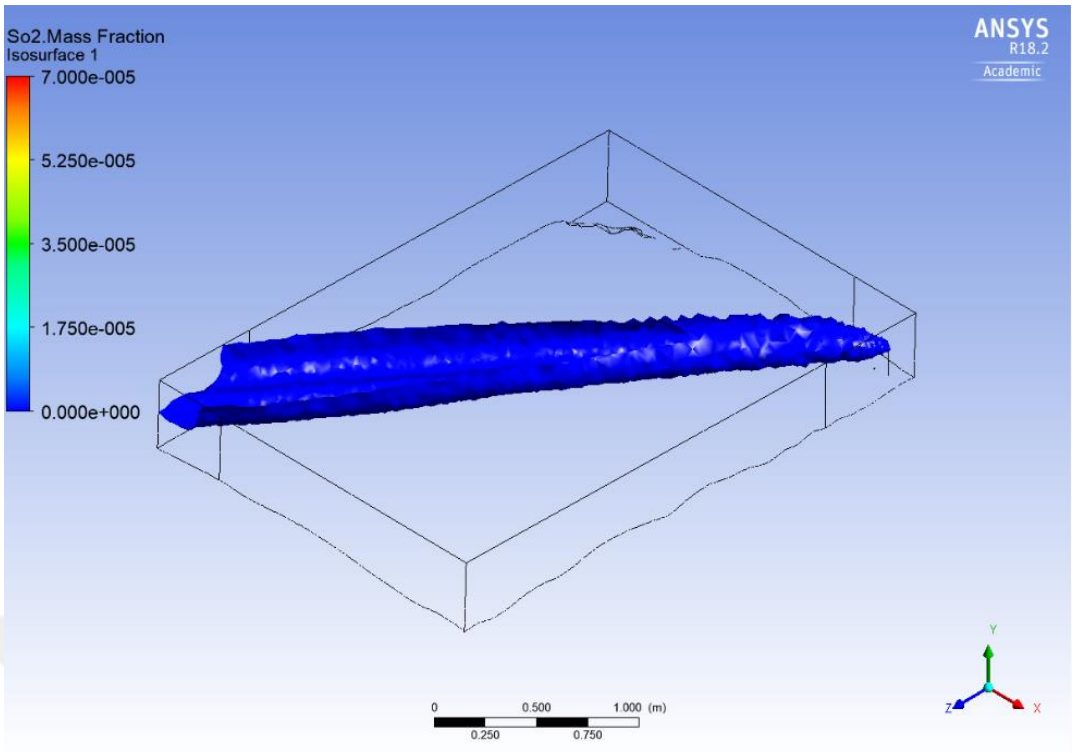

(f) Case 6 – 393 m (PBL height)

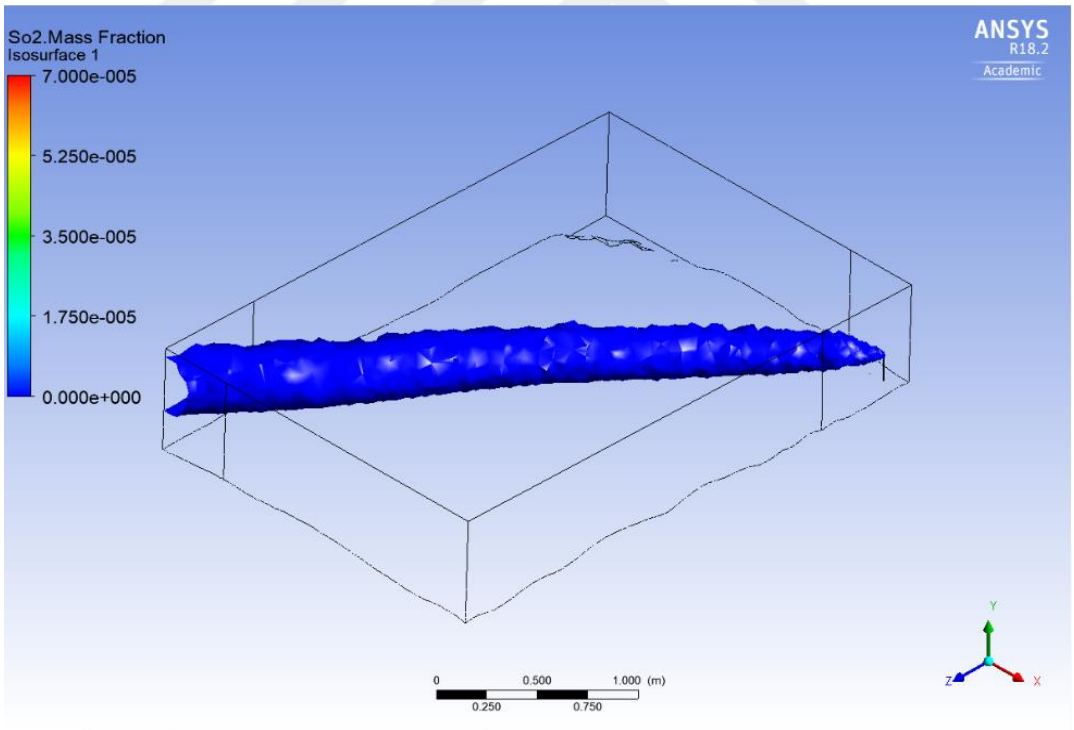

(g) Case 7 – 616 m (PBL height)

Figure 5.5 The CFD iso-surface plots based on SO_2 mass fraction for all cases

The seven cases in Figure 5.5 (a) to (g) were simulated under different wind speeds and different PBL heights. All geometries were reprepared for corresponding PBL heights. The pollutant concentrations were calculated at probe points that intersect the AQMS on the terrain map. The calculations were based on pollutant mass fraction. They were converted to ppm value by multiplying by 10^6. Then, mass/volume concentration was calculated according to Equation 5.1

$$\frac{mg}{m^3} = ppm\frac{PM_A}{RT} \tag{5.1}$$

The calculated concentrations are given in Table 5.2.

The behaviour of the plume implies that it is affected by the terrain geometry. It does not move straight from the source to the receptor point and makes curves depending on the shape of the terrain. In order to show this feature, we run the model for flat and elevated terrain in Ansys Fluent. A sample figure for one case is shown in Figure 5.6.

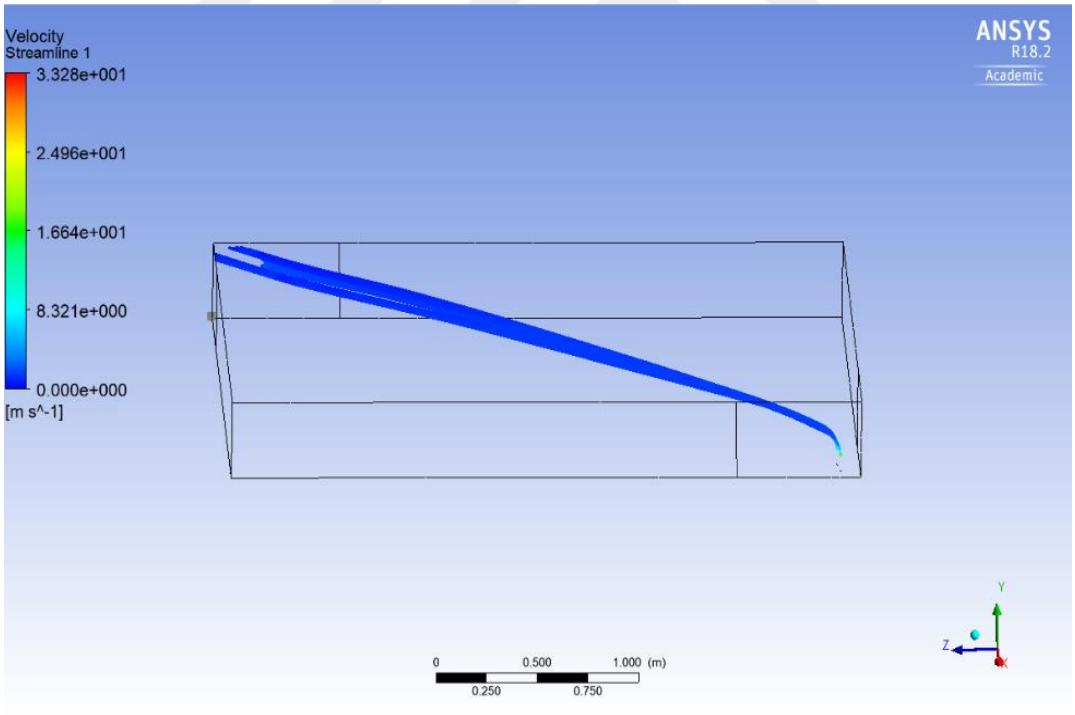

(a) 392 m (PBL height) (for flat terrain)

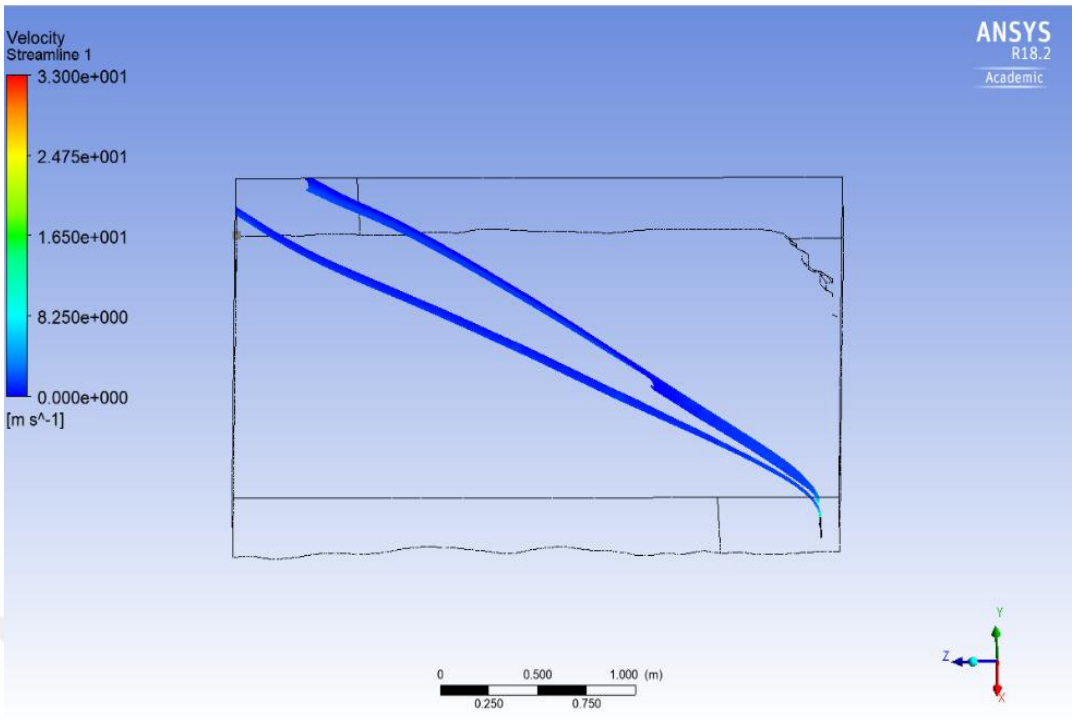

(b) 392 m (PBL height) (for elevated terrain)

Figure 5.6 Velocity streamline at different surface properties (a) for flat terrain (b) for elevated terrain

At low PBL heights, the plume cannot be lifted as it is in a high PBL case and this results in increased SO_2 concentrations at ground level. In the 1st, 2nd, and 3rd cases when the wind speed is low (1.5 m/s), the plume disperses more and causes a higher concentration at the ground level receptor point.

5.4 CFD and AERMOD Model Results Comparison

Table 5.2 shows AQMS measurement values and AERMOD and CFD estimated SO_2 concentrations at the receptor point. The concentration values downwind of the source are varied significantly between AERMOD and CFD simulations. Meteorological conditions, especially PBL, had a significant impact on predicted downwind SO_2 concentration in two different models. For all cases, AERMOD predicted higher values than CFD. In four cases AERMOD predicted higher than observation values, while in three cases the model predicted lower values compared to observation value. The higher estimated values were ranged from 10.3% to 42.4%. The reason for high estimation can be due to the effect of terrain in-situ cases. Figure 5.6 indicated that terrain effects impact the pollutant

trajectory. However, AERMOD assumes a straight path for the transport of pollutants. When CFD is executed in flat terrain case, the estimated cases were increased from 10.36, 5.55, and 2.00 to 20.42, 10.66, 4.44 μg/m^3, respectively. Although the model parameters are the same, the only difference is the terrain. In the hypothetical flat terrain, the concentrations were almost twice the real terrain options. This is attributed to increased path length and dispersion during the parcel movement from the stack to the source. CFD calculated lower downwind concentrations for all cases compared to station observed value.

Table 5.2 Comparison of Measurement and CFD and AERMOD estimated SO_2 concentration results

Case Number	Date-Hour	Wind Speed (m/s)	PBL Height (m)	Observation value (μg/m^3)	AERMOD results (μg/m^3)	CFD results (μg/m^3)
1	08.01.2014-11:00	1.5	392	16.1	22.93	10.36
2	08.01.2014-12:00	1.5	413	16	22.54	5.55
3	08.01.2014-13:00	1.5	427	16.3	17.98	2.00
4	13.03.2014-12:00	3.6	663	8.9	5.79	0.25
5	21.03.2014-08:00	5.7	333	8.7	4.82	0.39
6	27.03.2014-09:00	4.1	393	8.3	9.2	0.18
7	27.03.2014-12:00	5.7	616	8.2	3.02	0.04

A study, conducted by Kozić et al., (2015), by executing CFD to determine the dispersion of SO_2 from a power plant, calculated lower concentrations than measured values. It was attributed to the high temperature of the stack exit gas, the height of the stack, and other pollution sources. In contrast, Bonifacio et al., (2014) used AERMOD and CFD models to simulate the dispersion of particles emitted from area sources. According to their simulation results, the downwind concentrations calculated by AERMOD were lower than those calculated by CFD.

Other experiments, such as those by Blocken et al., (2008) and Demeal & Carissimo, (2008), found that CFD estimated higher concentrations than Gaussian-based atmospheric dispersion models.

According to the observation results, AERMOD and CFD, the highest concentration values were obtained at 1.5 m/s, which is the lowest wind speed. Fatahillah et al., (2020) reported similar results. They found lower SO_2 concentrations in the atmosphere when the wind speed around the source was higher. The effect of PBL was compared for the first three cases in Table 5.2 due to having the same wind speed. The highest concentration estimation was observed when PBL had the lowest value and the lowest concentration was observed when PBL had the highest value. This situation confirmed the effect of PBL on pollutant concentrations.

Riddle et al., (2004) used CFD to simulate gas dispersion from a single stack and compared the results with ADMS (Atmospheric Dispersion Modelling System) Gaussian dispersion model. They found satisfactory results with CFD simulations using Lagrangian particle tracking (LP) method but they recommended its use for complex geometries where ADMS doesn't calculate accurate results. Because CFD takes a long time to run and is difficult to set up.

Dourado et al., (2012) used AERMOD, CALPUFF, and CFD models to determine odor concentration. The estimations were verified by wind tunnel measurements. They reported that AERMOD and CALPUFF underestimated concentration values compared to CFD.

In another study, Kakosimos et al. (2011) used the numerical CFD model (steady-state Lagrangian model) and AERMOD to simulate the dispersion of PM from the overburden dumps of mine. They found that PM concentration levels are often underestimated by the CFD model and they stated that a good use of a CFD model in one case does not imply that it would work well in all situations. As a result, they suggested using both models to obtain a complete view.

Akyuz & Kaynak, (2019) calculated the combined impact of three operating and ten planned coal-fired power plants in Çanakkale for the same region and same year, utilizing the CALPUFF dispersion model. They performed three cases using a

different number of surface and radiosonde stations. Similar to our study, they reported that SO_2 emissions from the region's thermal power plants were transported to the district center to the south and south-west. They stated that AQMSs did not detect SO_2 emissions from thermal power plants. The estimated maximum daily SO_2 concentration at Biga-İçdaş station between 5.95-11.56 $\mu g/m^3$ for all coal-fired power plants. In our study, we calculated 24-hr maximum SO_2 concentration at Biga İçdaş as 7.89 $\mu g/m^3$ using AERMOD. When we compare the results, the calculated value is in the range calculated with the CALPUFF model.

There may be a disparity between model estimates and observations because the model can not account for all of the variables that make a change in observation results at a given time and place. Also, instrument errors, such as those caused by weather stations, may lead to the deviations between predicted and observed results (D'Abreton, 2009). The uncertainty caused by wind direction alone can trigger disappointing results from what appears to be a well-performing dispersion model, according to model developers' experience (Paine et al., 1998).

6
CONCLUSION

The aim of the study is to evaluate the dispersion of SO_2 in a real three-dimensional environment under different meteorological conditions using AERMOD and CFD models that have different approaches. To assess the accuracy of the models the CFD model was tested using seven different cases with varying wind speeds and PBL heights computed using AERMET, then the results compared with the AERMOD model results as well as to the observation values.

The three-dimensional terrain, changing meteorological conditions (varying wind speed and direction) have a major impact on flow and pollutant dispersion. To understand the effect on dispersion, the 3D geometry and PBL are considered in CFD simulations. According to the CFD simulation results, the model is capable of simulating the dispersion of SO_2, but calculated lower downwind concentrations for all seven cases compared to AERMOD and observation values. AERMOD predicted higher concentrations than observation values in four cases, while in three cases the model predicted lower values compared to the observation value. As this is not an expected case and seems like an erroneous incidence, we attributed this to the shortened distance of the estimation path in AERMOD. The principal difference between AERMOD and CFD relies on their methodologies. Since CFD has Eulerian based methodology, where AERMOD is a Gaussian dispersion model.

Although CFD needs geometry for each modelling hour, it has great potential in air quality modelling studies. Because the results of the study indicated the effect of real terrain properties in real studies. The modelling accuracy of CFD is increased when real terrain is used as the geometry of the model. We propose that CFD assisted with real terrain options especially in complex terrain geometries.

REFERENCES

Akyuz, E., & Kaynak, B. (2017). Çanakkale'de Kurulması Planlanan Kömür Yakıtlı Termik Santrallerin Hava Kirliliğine Katkısının Belirlenmesi.

Akyuz, E., & Kaynak, B. (2019). Use of dispersion model and satellite SO2 retrievals for environmental impact assessment of coal-fired power plants. *Science of the Total Environment*, *689*, 808–819. https://doi.org/10.1016/j.scitotenv.2019.06.464

Arya, S. P. (1999). *Air pollution meteorology and dispersion*.

Blocken, B., Stathopoulos, T., Saathoff, P., & Wang, X. (2008). Numerical evaluation of pollutant dispersion in the built environment: Comparisons between models and experiments. *Journal of Wind Engineering and Industrial Aerodynamics*, *96*(10–11), 1817–1831. https://doi.org/10.1016/j.jweia.2008.02.049

Bluett, J., N. Gimson, et al. (2004). *Good Practice Guide for Atmospheric Dispersion Modelling*.

Bonifacio, H. F., Maghirang, R. G., & Glasgow, L. A. (2014). Numerical simulation of transport of particles emitted from ground-level area source using AERMOD and CFD. *Engineering Applications of Computational Fluid Mechanics*, *8*(4), 488–502. https://doi.org/10.1080/19942060.2014.11083302

Chambers, L. A. (2013). Classification and extent of air pollution problems. In *Air Pollution Volume I*.

D'Abreton, P. (2009). Air Quality Modelling Best Practice Guidance for the Australian Alumina Industry" Queensland Environment consultants report prepared for Australian Aluminium Council.

Demeal, E., & Carissimo, B. (2008). Comparative evaluation of an Eulerian CFD and Gaussian plume models based on Prairie Grass dispersion experiment. *Journal of Applied Meteorology and Climatology*, *47*(3), 888–900. https://doi.org/10.1175/2007JAMC1375.1

Dourado, H., Santos, J., Reis, N., & Melo, A. M. V. (2012). The effects of atmospheric turbulence on peak-to-mean concentration ratio and its consequence on the odour impact assessment using dispersion models. *Chemical Engineering Transactions*, *30*, 163–168. https://doi.org/10.3303/CET1230028

Dudhia. (1989). Numerical study of convection observed during the Winter Monsoon Experiment using a mesoscale two-dimensional model. *Journal of the Atmospheric Sciences*, *46*(20), 3077–3107.

Dudhia, F. C. and J. (2001). Coupling an Advanced Land Surface – Hydrology Model with the Penn State – NCAR MM5 Modeling System . Part I : Model Implementation and Sensitivity. *Review, Monthly Weather*, 569–585.

EEA (European Environment Agency). (2014). *Air pollution fact sheet 2014: Belgium*. 28.

Fatahillah, A., Masyhudi, M. A., & Setiawan, T. B. (2020). Numerical analysis of air pollutant dispersion in steam power plant area using the finite volume method.

Journal of Physics: Conference Series, *1490*(1). https://doi.org/10.1088/1742-6596/1490/1/012002

Gemici Z., Kale O., Yuva H. ve Çaçan İ. (2017). Hava Kalitesi İzleme Sürecinde Yasal Yükümlülükler, VII. Ulusal Hava Kirliliği ve Kontrolü Sempozyumu, 1-3 Kasım, Antalya.

Henderson-Sellers, B. (1984). *Pollution of our Atmosphere*. Adam Hilger Ltd.

HKDYY. (2008). *Hava Kalitesinin Değerlendirilmesi ve Yönetimi Yönetmeliği*.

Holmes, N. S., & Morawska, L. (2006). A review of dispersion modelling and its application to the dispersion of particles: An overview of different dispersion models available. *Atmospheric Environment*, *40*(30), 5902–5928. https://doi.org/10.1016/j.atmosenv.2006.06.003

Içdaş. (2013). İçdaş Sürdürülebilirlik Raporu.

John H. Seinfeld and Sypros N. Pandis. (2006). *Atmospheric Chemistry and Physics: From Air Pollution to Climate Change*. John Wiley & Sons.

Kain, J. S. (2004). The Kain–Fritsch Convective Parameterization: An Update. *Journal of Applied Meteorology*, *1980*, 170–181.

Kakosimos, K. E., Assael, M. J., Lioumbas, J. S., & Spiridis, A. S. (2011). Atmospheric dispersion modelling of the fugitive particulate matter from overburden dumps with numerical and integral models. *Atmospheric Pollution Research*, *2*(1), 24–33. https://doi.org/10.5094/APR.2011.004

Karatzas, K. D., & Kaltsatos, S. (2007). Air pollution modelling with the aid of computational intelligence methods in Thessaloniki, Greece. *Simulation Modelling Practice and Theory*, *15*(10), 1310–1319. https://doi.org/10.1016/j.simpat.2007.09.005

Kesarkar, A. P., Dalvi, M., Kaginalkar, A., & Ojha, A. (2007). Coupling of the Weather Research and Forecasting Model with AERMOD for pollutant dispersion modeling. A case study for PM10 dispersion over Pune, India. *Atmospheric Environment*, *41*(9), 1976–1988. https://doi.org/10.1016/j.atmosenv.2006.10.042

Kozić, M. S., Ristić, S. S., Štetić Kozić, S. M., & Polić, S. R. (2015). A numerical study for the assessment of pollutant dispersion from kostolac b power plant to viminacium for different atmospheric conditions. *Thermal Science*, *9*(2), 425–434. https://doi.org/10.2298/TSCI130115158K

Kumar, A., Patil, R. S., Dikshit, A. K., & Kumar, R. (2017). Application of WRF model for air quality modelling and AERMOD – A survey. *Aerosol and Air Quality Research*, *17*(7), 1925–1937. https://doi.org/10.4209/aaqr.2016.06.0265

Lee, C. Y., & Zhou, P. (2015). Directional shadow price estimation of CO2, SO2 and NOx in the United States coal power industry 1990-2010. *Energy Economics*, *51*(x), 493–502. https://doi.org/10.1016/j.eneco.2015.08.010

Leelőssy, Á., Molnár, F., Izsák, F., Havasi, Á., Lagzi, I., & Mészáros, R. (2014). Dispersion modeling of air pollutants in the atmosphere: a review. *Central European Journal of Geosciences*, *6*(3), 257–278.

https://doi.org/10.2478/s13533-012-0188-6

Lettau, H. H. (1970). *Physical and meteorological basis for mathematical models of urban diffusion processes*.

Li, L., Chen, C., Xie, S., Huang, C., Cheng, Z., Wang, H., Wang, Y., Huang, H., Lu, J., & Dhakal, S. (2010). Energy demand and carbon emissions under different development scenarios for Shanghai, China. *Energy Policy*, *38*(9), 4797–4807. https://doi.org/10.1016/j.enpol.2009.08.048

Malakan, W., Keawboonchu, J., & Thepanondh, S. (2018). Comparison of AERMOD performance using observed and prognostic meteorological data. *EnvironmentAsia*, *11*(2), 38–52. https://doi.org/10.14456/ea.2018.21

MARKA. (2012). *Green Kocaeli-Gelişmiş Rehabilite ve Endüstriyel Nüanslarla Kocaeli'de Çevre Konsepti Çalıştay Kitabı, Kocaeli Çevre ve Şehircilik İl Müdürlüğü, Doğu Marmara Kalkınma Ajansı*.

Mlawer, E. J., Taubman, J., Brown, P. D., Iacono, M. J., & Clough, S. A. (1997). *Radiative transfer for inhomogeneous atmospheres: RRTM, a validated correlated-k model for the longwave*. *102*.

Nam, K. M., Waugh, C. J., Paltsev, S., Reilly, J. M., & Karplus, V. J. (2013). Carbon co-benefits of tighter SO2 and NOx regulations in China. *Global Environmental Change*, *23*(6), 1648–1661. https://doi.org/10.1016/j.gloenvcha.2013.09.003

NAQMN. https://www.havaizleme.gov.tr/

Omidvarborna, H., Kumar, A., & Kim, D. S. (2015). Recent studies on soot modeling for diesel combustion. *Renewable and Sustainable Energy Reviews*, *48*, 635–647. https://doi.org/10.1016/j.rser.2015.04.019

Paine, R.J., R.F. Lee, R. Brode, R.B. Wilson, A.J. Cimorelli, S.G. Perry, J.C.Weil, A. Venkatram, and W. D. P. (1998). *Model evaluation results for AERMOD (draft document)*.

Pasquill, F. (1971). Atmospheric dispersion of pollution. *Quarterly Journal of the Royal Meteorological Society*, *97*(414), 369–395. https://doi.org/10.1002/qj.49709741402

Riddle, A., Carruthers, D., Sharpe, A., McHugh, C., & Stocker, J. (2004). Comparisons between FLUENT and ADMS for atmospheric dispersion modelling. *Atmospheric Environment*, *38*(7), 1029–1038. https://doi.org/10.1016/j.atmosenv.2003.10.052

Sharma, N., Chaudhry, K. K., & Chalapati Rao, C. V. (2004). Vehicular pollution prediction modelling: A review of highway dispersion models. *Transport Reviews*, *24*(4), 409–435. https://doi.org/10.1080/0144164042000196071

Shourangiz-Haghighi, A., Haghnegahdar, M. A., Wang, L., Mussetta, M., Kolios, A., & Lander, M. (2020). State of the Art in the Optimisation of Wind Turbine Performance Using CFD. *Archives of Computational Methods in Engineering*, *27*(2), 413–431. https://doi.org/10.1007/s11831-019-09316-0

Singh, J., Srikanth, R., & Ramasesha, S. K. (2020). *Dispersion of Particulate Matter and Sulphur Oxides from Thermal Power Plant : A case study*. *July*, 1–21.

https://doi.org/10.20944/preprints202007.0231.v1

Sinha, N., Ghose, M. K., Singh, G., Srivastava, S., & Sinha, I. N. (2004). Classification of Air Pollution Dispersion Models : a Critical Review. *Proceedings of the National Seminar on Environmental Engineering with Special Emphasis on Mining Environment*, *April*, 2004–2019.

Streeter, J. L. (2016). Adoption of SO2 emission control technologies - An application of survival analysis. *Energy Policy*, *90*, 16–23. https://doi.org/10.1016/j.enpol.2015.11.035

Suerdem, T. B., & Yildirim, I. (2009). Fungi in the atmospheric air of Çanakkale province in Turkey. *African Journal of Biotechnology*, *8*(18), 4450–4458. https://doi.org/10.4314/ajb.v8i18.62399

Thi Nguyen, H., & Kim, K. H. (2006). Evaluation of SO2 pollution levels between four different types of air quality monitoring stations. *Atmospheric Environment*, *40*(36), 7066–7081. https://doi.org/10.1016/j.atmosenv.2006.06.011

TUIK. (2020). *No Title*. http://www.tuik.gov.tr

U.S. EPA. (2004). *User's Guide for the AERMOD Meteorological Preprocessor (AERMET). Office of Air Quality Planning and Standards*.

U.S. EPA. (2019). *AERMOD Implementation Guide*.

Weber, E. (1982). *Air Pollution: Assessment Meteorology and Modelling.* Plenum Press.

WHO. (2016). Ambient (outdoor) air quality and health.

Willmott, C. J. (1982). Some comments on the evaluation of model performance. *Bulletin - American Meteorological Society*, *63*(11), 1309–1313. https://doi.org/10.1175/1520-0477(1982)063<1309:SCOTEO>2.0.CO;2

Zou, B., Wilson, J. G., Zhan, F. B., & Zeng, Y. (2009). Spatially differentiated and source-specific population exposure to ambient urban air pollution. *Atmospheric Environment*, *43*(26), 3981–3988. https://doi.org/10.1016/j.atmosenv.2009.05.022

A

WPS INPUT

```
&share
 wrf_core = 'ARW',
 max_dom = 2,
 start_date = '2014-01-01_00:00:00','2014-01-01_00:00:00',
 end_date   = '2014-02-01_00:00:00','2014-02-01_00:00:00',
 interval_seconds = 3600
 io_form_geogrid = 2,
/

&geogrid
 parent_id         =   1, 1,
 parent_grid_ratio =   1, 3,
 i_parent_start    =   1, 11,
 j_parent_start    =   1, 11,
 e_we              =  29, 25,
 e_sn              =  29, 25,
 geog_data_res = 'default','default',
 dx = 10000,
 dy = 10000,
 map_proj = 'lambert',
 ref_lat   =  40.25,
 ref_lon   =  27.06,
 truelat1  =  30.0,
 truelat2  =  60.0,
 stand_lon =  28.0,
 geog_data_path = '../WPS_GEOG/'
/

&ungrib
 out_format = 'WPS',
 prefix = 'FILE',
/

&metgrid
 fg_name = 'FILE'
 io_form_metgrid = 2,
/
```

B

WRF INPUT

```
&time_control
 run_days                 = 0,
 run_hours                = 744,
 run_minutes              = 0,
 run_seconds              = 0,
 start_year               = 2014, 2014,
 start_month              = 01, 01,
 start_day                = 01, 01,
 start_hour               = 00, 00,
 end_year                 = 2014, 2014,
 end_month                = 02, 02,
 end_day                  = 01, 01,
 end_hour                 = 00, 00,
 interval_seconds         = 3600
 input_from_file          = .true., .true.,
 history_interval         = 60, 60,
 frames_per_outfile       = 1000, 1000,
 restart                  = .false.,
 restart_interval         = 7200,
 io_form_history          = 2,
 io_form_restart          = 2,
 io_form_input            = 2,
 io_form_boundary         = 2,
 /
 &domains
 time_step                = 180,
 time_step_fract_num      = 0,
 time_step_fract_den      = 1,
 max_dom                  = 2,
 e_we                     = 29, 25,
```

```
e_sn                          = 29, 25,
e_vert                        = 33, 33,
p_top_requested               = 5000,
num_metgrid_levels            = 27,
num_metgrid_soil_levels       = 4,
dx                            = 10000, 3333.33325,
dy                            = 10000, 3333.33325,
grid_id                       = 1,    2,
parent_id                     = 0,    1,
i_parent_start                = 1,    11,
j_parent_start                = 1,    11,
parent_grid_ratio             = 1,    3,
parent_time_step_ratio        = 1,    3,
feedback                      = 1,
smooth_option                 = 0
/
&physics
mp_physics                    = 4,    4,
cu_physics                    = 1,    1,
ra_lw_physics                 = 1,    1,
ra_sw_physics                 = 1,    1,
bl_pbl_physics                = 1,    1,
sf_sfclay_physics             = 1,    1,
sf_surface_physics            = 4,    4,
radt                          = 30,   30,
bldt                          = 0,    0,
cudt                          = 0,    0,
icloud                        = 1,
num_land_cat                  = 21,
sf_urban_physics              = 0,    0,
/
&fdda
/
```

```
&dynamics
hybrid_opt                = 2,
w_damping                 = 0,
diff_opt                  = 1,     1,     1,
km_opt                    = 4,     4,     4,
diff_6th_opt              = 0,     0,     0,
diff_6th_factor           = 0.12,  0.12,  0.12,
base_temp                 = 290.
damp_opt                  = 3,
zdamp                     = 5000., 5000., 5000.,
dampcoef                  = 0.2,   0.2,   0.2
khdif                     = 0,     0,     0,
kvdif                     = 0,     0,     0,
non_hydrostatic           = .true., .true., .true.,
moist_adv_opt             = 1,     1,     1,
scalar_adv_opt            = 1,     1,     1,
gwd_opt                   = 1,
/
&bdy_control
spec_bdy_width            = 5,
specified                 = .true.
/
&grib2
/
&namelist_quilt
nio_tasks_per_group       = 0,
nio_groups                = 1,
```

PUBLICATIONS FROM THE THESIS

Conference Papers

1. Yavuz E., Kuzu S. L., Saral A., Suphur dioxide emission dispersion modelling from a coal fired power plant in Çanakkale, Turkey, 5th EURASIA Waste Management Symposium, 26-28 October, 2020.